

INFORMATION TO USERS

This was produced from a copy of a document sent to us for microfilming. While the most advanced technological means to photograph and reproduce this document have been used, the quality is heavily dependent upon the quality of the material submitted.

The following explanation of techniques is provided to help you understand markings or notations which may appear on this reproduction.

1. The sign or "target" for pages apparently lacking from the document photographed is "Missing Page(s)". If it was possible to obtain the missing page(s) or section, they are spliced into the film along with adjacent pages. This may have necessitated cutting through an image and duplicating adjacent pages to assure you of complete continuity.
2. When an image on the film is obliterated with a round black mark it is an indication that the film inspector noticed either blurred copy because of movement during exposure, or duplicate copy. Unless we meant to delete copyrighted materials that should not have been filmed, you will find a good image of the page in the adjacent frame.
3. When a map, drawing or chart, etc., is part of the material being photographed the photographer has followed a definite method in "sectioning" the material. It is customary to begin filming at the upper left hand corner of a large sheet and to continue from left to right in equal sections with small overlaps. If necessary, sectioning is continued again—beginning below the first row and continuing on until complete.
4. For any illustrations that cannot be reproduced satisfactorily by xerography, photographic prints can be purchased at additional cost and tipped into your xerographic copy. Requests can be made to our Dissertations Customer Services Department.
5. Some pages in any document may have indistinct print. In all cases we have filmed the best available copy.

University
Microfilms
International

300 N. ZEEB ROAD, ANN ARBOR, MI 48106
18 BEDFORD ROW, LONDON WC1R 4EJ, ENGLAND

7908836

RENFRO, GEORGE MICHAEL
OPTICALLY STIMULATED EXOELECTRON EMISSION
FROM POTASSIUM-CHLORIDE SINGLE CRYSTALS.

THE UNIVERSITY OF OKLAHOMA, PH.D., 1978

University
Microfilms
International 300 N. ZEEB ROAD, ANN ARBOR, MI 48106

© 1979

GEORGE MICHAEL RENFRO

ALL RIGHTS RESERVED

THE UNIVERSITY OF OKLAHOMA

GRADUATE COLLEGE

OPTICALLY STIMULATED EXOELECTRON EMISSION
FROM POTASSIUM CHLORIDE SINGLE CRYSTALS

A DISSERTATION

SUBMITTED TO THE GRADUATE FACULTY

in partial fulfillment of the requirements for the

degree of

DOCTOR OF PHILOSOPHY

By

GEORGE MICHAEL RENFRO

Norman, Oklahoma

1978

OPTICALLY STIMULATED EXOELECTRON EMISSION
FROM POTASSIUM CHLORIDE SINGLE CRYSTALS

APPROVED BY

Michael J. Finkbeiner

Michael R. Manno

David W. Anderson

Stephen Whitmore

Robert J. Pety

DISSERTATION COMMITTEE

ACKNOWLEDGEMENTS

The author wishes to express his very deep appreciation to Professor Helmut Fischbeck for his help and guidance throughout this experiment and particularly for his encouragement during difficult times. This work would have been impossible without the understanding and support of the author's wife, Dianne. Significant financial support was provided by Mr. and Mrs. George M. Renfro and Dr. and Mrs. Forrest W. Olson.

Appreciation is due to Gerald Haddad and Thomas Rhymes for discussions concerning electronics and computer problems, and also to Gene Scott, Woody Porter and Wayne Ramsey for their patient and careful machine work during construction of the instruments.

TABLE OF CONTENTS

	Page
LIST OF TABLES	vi
LIST OF ILLUSTRATIONS.	vii
 Chapter	
I. INTRODUCTION	1
A. History.	1
B. Theory of Exoelectron Emission	4
1. Defect Formation	4
2. Luminescence of Color Centers.	5
3. Electron Emission From Color Centers	11
C. Statement of Purpose	12
II. APPARATUS.	15
A. Vacuum System.	15
B. Sample Holder.	15
C. Electron Gun	17
D. Electron Detector.	19
E. Optical System	21
III. DATA COLLECTION METHOD	24
IV. RESULTS.	31
V. DISCUSSION	58
REFERENCES	68

Appendix

1. Presetable Up/Down Counter	71
2. Voltage Controlled Oscillator.	74
3. Monostable Data Gate	79
4. TTL Relay.	83
5. Data Analysis Programs	85
6. Temperature Controller	94

LIST OF TABLES

Table	Page
1. Change of Emission and Absorption with Light Exposure. . . .	54
2. Voltage-to-Frequency Converter	76
3. Monostable Gate Parts List	82
4. Data Transfer Program.	88
5. Data Normalization Program	91

LIST OF ILLUSTRATIONS

Figure	Page
1. Fluorescence and Phosphorescence	7
2. Configuration Coordinate Diagram of F-Center	7
3. Absorption and Emission Spectrum of Alkali Halide.	9
4. Models of Thermoluminescence	10
5. Sample Holder.	16
6. Schematic of Experiment.	18
7. Charge Sensitive Pre-Amplifier	20
8. Electronics Block Diagram of Experiment.	23
9. Emission Spectrum of Xenon Lamp.	29
10. Response of Photomultiplier.	29
11. Exoemission and Absorption of KCl Crystal.	32
12. Comparison of Exoemission from Crystals and Powder	36
13. Exoemission of Crystal 1 versus Dose	37
14. Exoemission of Crystal 2 versus Dose	38
15. Exoemission at 75°C.	41
16. Exoemission at 60°C.	42
17. Exoemission at 45°C.	43
18. Exoemission at 30°C.	44
19. Exoemission versus External Magnetic Field	47
20. Exoemission versus Earth's Magnetic Field.	48

Figure	Page
21. Exoemission versus Scan Direction.	49
22. Exoemission versus Scan Number (red-to-blue)	52
23. Exoemission versus Scan Number (blue-to-red)	53
24. Exponential Fits to Exoemission Decay.	55
25. Freehand Fits to Exoemission Decay	56
26. Exoemission and Absorption Decay Data.	57
27. Proposed Energy Level Scheme	60
28. Presetable Up/Down Counter	72b
29. Counter Logic Circuit.	73
30. Voltage Controlled Oscillator Circuit.	75
31. Raytheon RM4151 V-to-F Chip.	77
32. Monostable Data Gate	81
33. TTL Relay Circuit.	84
34. Temperature Controller Block Diagram	95
35. Thermocouple Amplifier Circuit	96
36. Linear Ramp Circuit.	98
37. Zero Voltage Switch Circuit.	101

OPTICALLY STIMULATED EXOELECTRON EMISSION FROM POTASSIUM CHLORIDE SINGLE CRYSTALS

CHAPTER I INTRODUCTION

History

Stimulated exoelectron emission refers to the emission of low energy electrons from insulating surfaces when stimulated by heat or light. Thermally stimulated exoelectron emission (TSEE) occurs at temperatures well below the threshold for thermionic emission, and optically stimulated emission (OSEE) occurs at photon energies much lower than those required for the normal photoelectric effect. Exoemission has been observed in many insulating materials including minerals, ceramics, glasses, metal oxides and semiconductors, but it is most pronounced in the alkali halide crystals. In the alkali halides the effect may be bleached away by prolonged exposure to white light or annealed by heating the crystal to a few hundred degrees centigrade. The emission can then be re-induced by exposing the crystal to ionizing radiation.

The first detailed investigation of exoelectrons was reported by McLennan in 1901.¹ He excited various salts with electrons and then allowed the emitted particles from the salt sample to discharge an electrometer. In this way he established that the emitted particles were negatively charged and that in many cases there was a relationship

between the exoemission and thermoluminescence.

In the 1930's it was found that an abnormally high background counting rate occurred in newly manufactured Geiger counter tubes. This was attributed to exoemission from the oxide coatings of newly machined metal parts. However it was not until the 1950's that detailed studies of TSEE and OSEE were begun. In 1950 Apker and Taft reported an OSEE peak which occurred at the same wavelength as the alpha absorption band in potassium iodide.² In 1952 Kramer published results of a TSEE study which established that exoelectrons are emitted in well defined emission peaks occurring at different temperatures.³

From the 1950's until the present, research in exoemission has divided itself into the two disciplines of thermally stimulated emission and optically stimulated emission. TSEE studies have received the majority of the research effort due to their close correlation with thermoluminescence effects which are of interest as a dosimetry technique. The fields of thermoluminescence and TSEE as they relate to dosimetry were recently reviewed by Becker.⁴

Becker states that exoemission has been observed under many circumstances such as: (1) after the deformation or abrasion of metal oxides, minerals, or ionic crystals, (2) during changes in crystal structure, (3) during chemical reactions, and (4) after exposure to ionizing radiation. Thermally stimulated emission peaks may occur at temperatures ranging from -240° C to 600° C. After exposure to radiation many materials display an "after emission" which decreases exponentially with time. This after emission requires no stimulation energy other than the heat available to the system at room temperature. Measurements of the

kinetic energies of exoelectrons have been hampered by the problems of sample charging, but energies are generally thought to be less than 1eV.⁵

It seems apparent that the phenomenon referred to as exoelectron emission is really several, if not many, different phenomena which all result in the emission of electrons under conditions which cannot be explained by the normal photoeffect or by thermionic emission. In fact it was demonstrated by DeMuer and Maenhout that the particles responsible for TSEE peaks in ZnO are not electrons at all, but negative ions.⁶ Among the ionic crystals where the emitted particles are thought to be electrons it was demonstrated by Gordan and Scharmann that some emission peaks are related to absorbed gasses while others are related to crystal lattice defects such as color centers.⁷

Optically stimulated exoelectron emission was first noticed as a shifting of the photoelectron emission edge to longer wavelengths. This phenomenon was referred to as the "external photoeffect" and was reported by Lukirsky et al. in 1926⁸ and by Fleishmann in 1933.⁹ When Apker and Taft reported the correlation between OSEE and the alpha absorption band in 1950 investigations were started by Bohun^{10,11} and by Sujak¹² culminating in a series of papers by Petrescu¹³⁻¹⁶ in which the OSEE peaks were correlated with the optical absorption of F, M and R color centers in many of the alkali halides.

In these early investigations samples were irradiated with low energy (less than 10 keV) electron beams and then placed into a gas flow counter where they could be stimulated by light from a monochromator and their exoemission could be recorded. Petrescu reported that the observed emission rate was very small, on the order of 50 counts per second, and

there was often difficulty in reproducing the emission peaks.¹⁴ Because of the low emission intensity he did not correct the emission spectra to account for the spectral shape of his light source.¹³ Polycrystalline layers of salt precipitated or melted onto a metal substrate were used as samples rather than single crystals.¹⁰⁻¹⁶ Petrescu reported that sometimes emission peaks were observed that had no relationship to the published color center levels, and sometimes only an emission edge was observed--similar to the "external photoeffect."¹⁴

Since many of the exoemission phenomena are resonance-like effects displaying definite emission peaks as a function of stimulation energy, and since some exoelectrons are thought to be related to trapping centers associated with the crystal lattice, it appears that optically stimulated exoemission studies may be a most promising method for studying these phenomena.

Theory of Exoelectron Emission

Exoemission probably results from several different phenomena including adsorbed gasses, lattice defects, and photodesorption of ions. This paper will be concerned with lattice defects. The exoemission process associated with defects or color centers consists of three phases each of which constitutes an area of research in its own right. These are: (1) the creation of defects by ionizing radiation, (2) the emission of electrons from trapping centers, (3) the bleaching (or annealing) of traps.

Defect Formation

It has been known since the 1950's that color centers can be formed in alkali halide crystals by bombarding with ultraviolet photons

of energies greater than about 10 eV or with electrons in the energy range 10^2 - 10^3 eV. This is surprising since the typical energies required to displace a halogen ion from its lattice site are around 25 eV. Conservation of momentum would require an electron to have about 4×10^5 eV in order to displace a chlorine ion by direct collision.¹⁷ Several models have been proposed to explain low energy defect formation. These are discussed by Townsend and Kelly.¹⁸

A model proposed by Pooley¹⁹ and Hersh²⁰ has had the greatest success in accounting for experimental results. According to this model bound electron-hole pairs (excitons) are produced by the incident radiation and subsequently become trapped at a molecular halide ion in the lattice. This forms an excited system in which the electron and hole attempt to re-combine. De-excitation can result in a radiative transition (luminescence) at low temperatures, but at sufficiently high temperatures the decay may be non-radiative and the exciton energy will be transferred to the ion pair resulting in lattice displacements. The name given to the defect in which a halide is removed from its lattice position is the "alpha center". When an electron becomes trapped at the halogen vacancy the alpha center becomes an "F-center". It should be noted that according to the Pooley model the exciton involved in the defect formation loses its energy to the halogen ions without recombining. Thus one expects a direct formation of F-centers containing an electron in its ground state.

Luminescence of Color Centers

Since the models that have been proposed for exoelectron emission from color centers are closely related to the processes of fluorescence

and thermoluminescence it is best to review the models for the luminescent effects before proceeding. The term "luminescence" will be used to refer to the emission of light by any process other than incandescence. There are three types of luminescence which should be distinguished: fluorescence, phosphorescence and thermoluminescence.

As shown in Figure 1 the processes of fluorescence and phosphorescence involve transitions between ground and excited states of a luminescent center or "activator". Fluorescence is a direct and spontaneous radiative decay from the excited to the ground state. Phosphorescence occurs when an electron has been excited into a metastable state from which the ground state transition is forbidden. In this case activation energy such as heat or light must be supplied by an external source in order to raise the electron into a higher excited state from which the ground state transition is allowed. Thus in the case of phosphorescence the decay time depends upon the temperature of the system while in the case of fluorescence it does not.

The luminescent center or color center may be represented on a configuration coordinate diagram as shown in Figure 2. The minimum on the bottom parabola represents the equilibrium position of the center, while higher points on the curve represent vibrational levels. The upper parabola represents the first electron excited state of the center. In the excited state the interatomic forces of neighboring atoms are usually weaker so the curvature of this state is less than that of the ground state and its minimum is displaced.

According to the Franck-Condon principle electronic transitions occur on time scales much shorter than lattice relaxations, so electronic

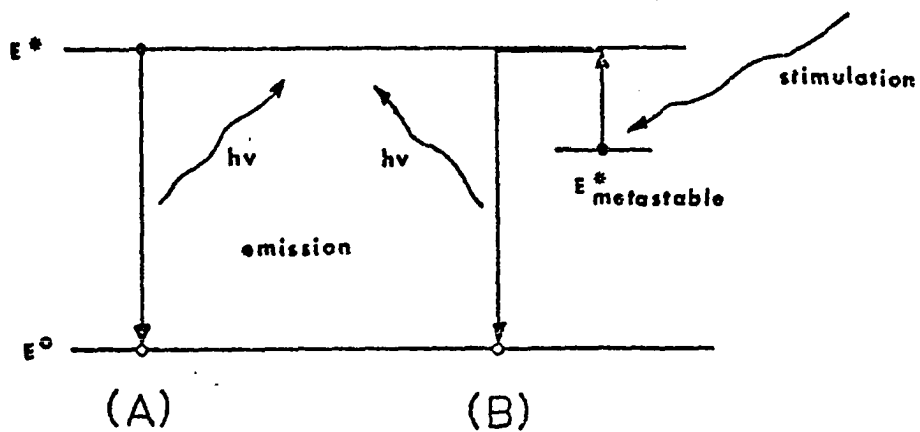


Figure 1. (A) Fluorescence, and
(B) Phosphorescence.

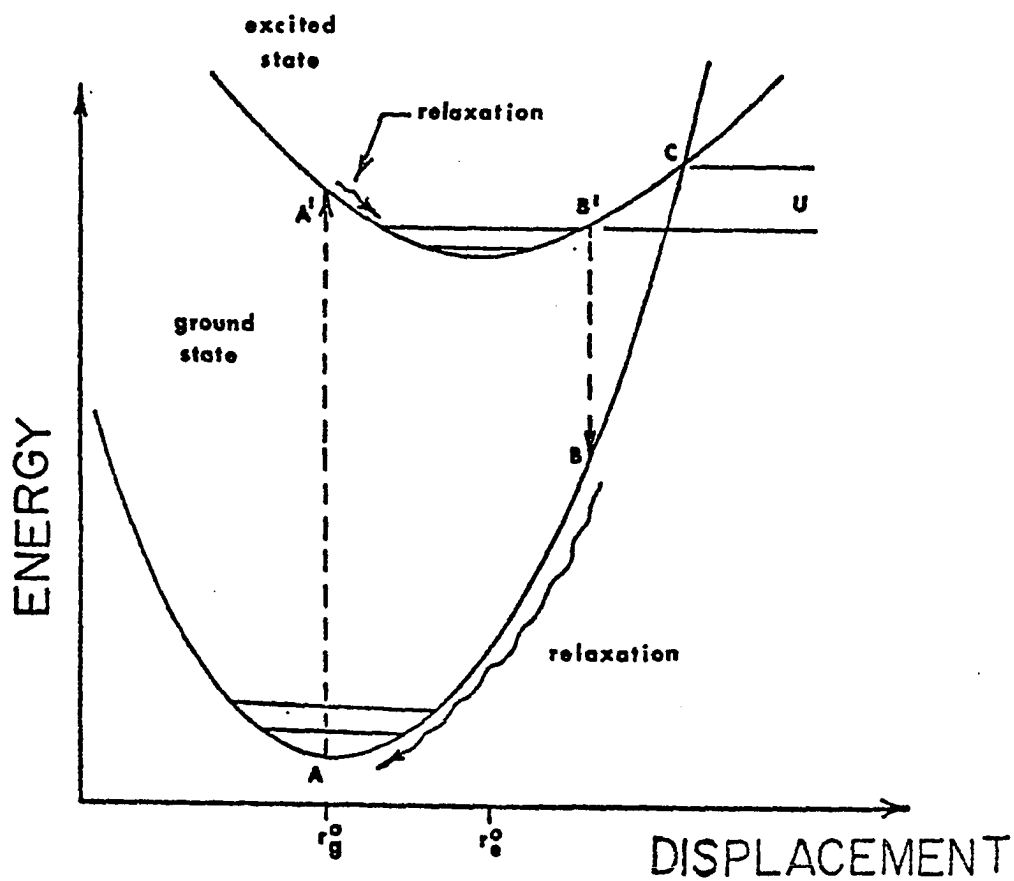


Figure 2. Configuration coordinate diagram of the F-center.

transitions are represented as vertical lines. When a quantum of energy is absorbed at A the electron will transfer to position A' in the excited state and then give up its excess vibrational energy as lattice phonons. During this process the excited center relaxes to point B' from which the electron can decay to the ground state. The photon emitted in the decay process is necessarily of lower energy than the one which was absorbed (Stokes' Shift). Once the electron has decayed to point B it can again lose energy to lattice phonons and the center will relax to its original configuration.

It should be noted that the ground state and excited state energy levels cross at point C thus making non-radiative transitions possible if enough activation energy, U , is supplied to the excited electron. Luminescent centers with small values of U are referred to as "killer" or "poison" centers because they increase the probability of non-radiative decay and thus kill the luminescence effect.

In the alkali halides the most common luminescence center is the F-color center. The excitation of the electron trapped at the halogen vacancy produces the F absorption band in the visible region of the optical spectrum and is responsible for the distinctive color of a damaged crystal. De-excitation of the center produces an infrared luminescence. In addition to the F-band other optical absorption bands are observed to the short wavelength side. These are labelled K, L_1 , L_2 , L_3 in Figure 3 and are thought to correspond to excitations of the trapped electron into higher excited states of the color center.²¹

Two classes of trapping centers exist in alkali halide crystals: (1) centers which trap electrons, and (2) centers which trap holes. As

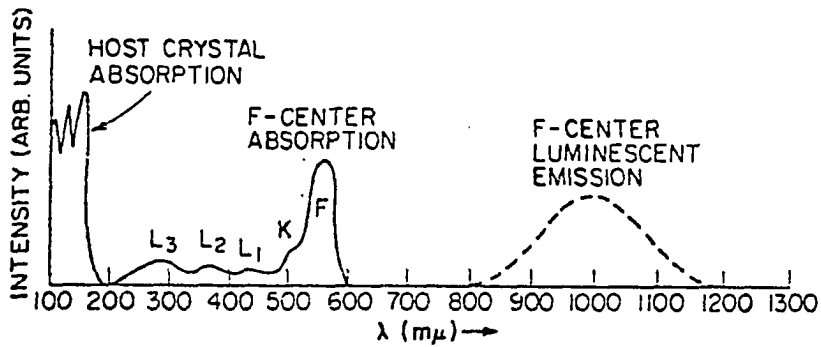


Figure 3. Typical absorption and luminescence spectrum of an alkali halide crystal.

previously mentioned lattice vacancies can exist in an ionized state in which no charge is trapped--in the case of a halogen vacancy the ionized center is the alpha center. It is apparent that the normal luminescence scheme of Figure 2 does not apply to the ionized center, and it no longer functions as an optical absorber or emitter. The model proposed by Randall and Wilkins to explain thermoluminescence is based upon the ionization of color centers.²²

The Randall-Wilkins model assumes that both electron and hole traps exist in the crystal. These traps may be normal lattice defects or impurity ions. As previously mentioned ionizing radiation incident on the crystal produces excitons. These excitons may dissociate and release energy to the lattice producing new defects, or as shown in Figure 4(A) they may become trapped at existing defects. A fraction of the released electrons will recombine and emit luminescence. The remainder will become trapped and find themselves in a metastable state where they may remain for long periods of time.

De-population of the traps can occur by three paths. If sufficient stimulation energy in the form of heat or light is supplied to the

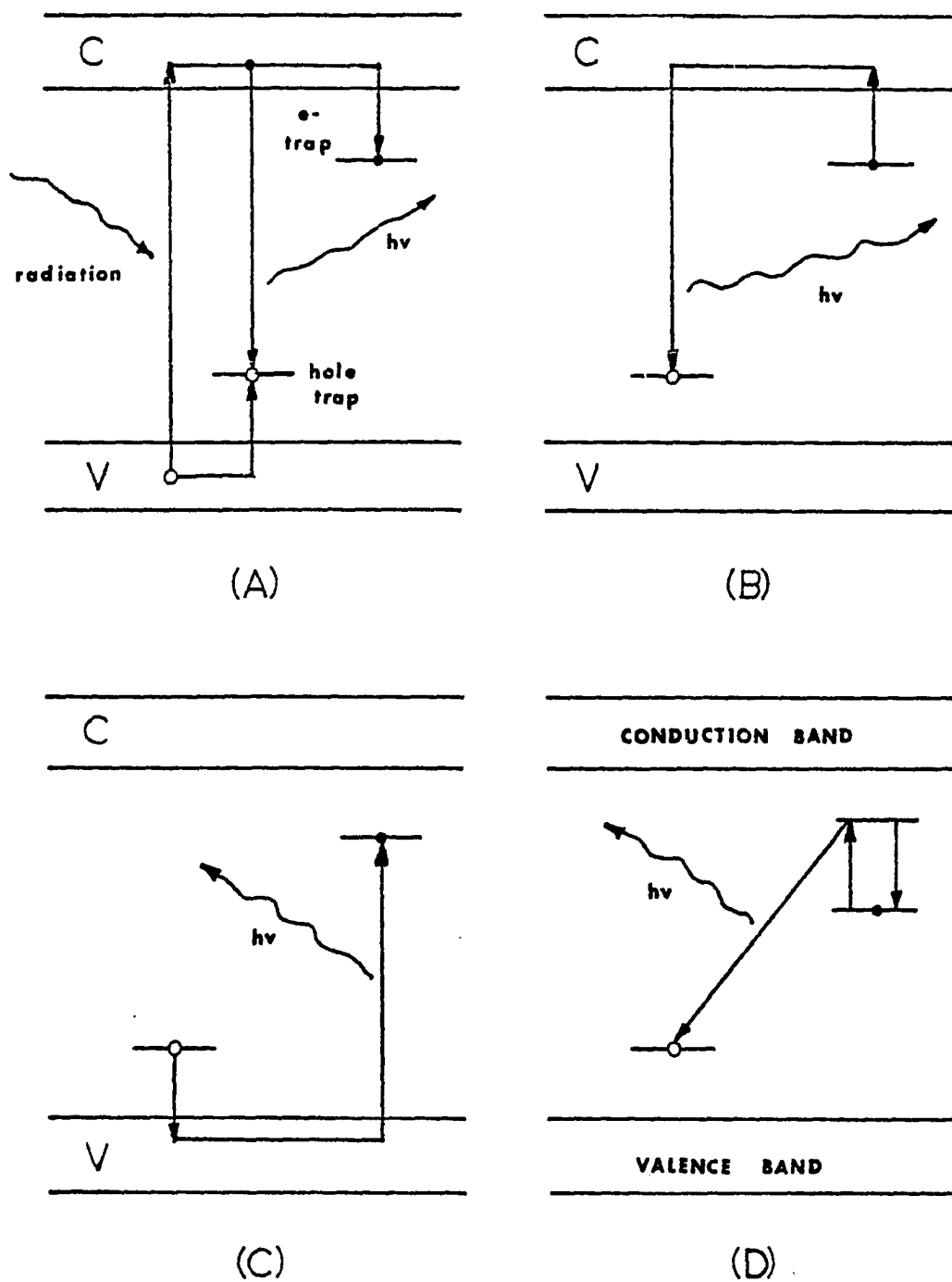


Figure 4. Models of thermoluminescence: (A) incident radiation creates trapped electron and hole, (B) freed electron recombines, (C) freed hole recombines, (D) excited electron recombines.

crystal the trapped electron may be promoted out of its trapping center and into the conduction band where it is free to re-combine with the trapped hole and emit a thermoluminescence photon as shown in Figure 4(B). Alternatively the stimulation energy may free the trapped hole to move through the crystal until it can combine with a trapped electron and emit light (Figure 4(C)). And finally, if the trapped electron is stimulated to an excited state of the trapping center, it may be possible for it to re-combine directly with a trapped hole and emit its excess energy.

Electron Emission from Color Centers

At least five different mechanisms have been proposed to explain how electrons can be emitted from a crystal under circumstances similar to the thermoluminescence process. These models were summarized by Bohun.²³ Each is briefly described below. For simplicity we will assume all electron traps to be F-centers.

(1) Direct ionization of the F-center. The electron is given sufficient stimulation energy to escape directly from the F-center into the vacuum. This process would be expected to require a stimulation energy greater than the F-center absorption band but less than the band gap energy, and should produce an emission edge similar to the photoelectric effect. The emission should cease as the F-centers are destroyed. This may be a mechanism responsible for the "external photoeffect".

(2) Maxwell tail emission. The stimulation energy may raise the trapped electron to the conduction band where it may either pick up enough thermal energy to escape or else give up some of its energy to another conduction electron which will then have enough energy to escape. Likewise this model should require stimulation energy between the F-center

absorption band and the band gap, and should produce an emission peak whose width is comparable to the width of the conduction band.

(3) Exciton enhanced emission. If the stimulation energy is near to or greater than the band gap it may produce excitons. The dissociation of excitons at F-centers may release enough energy to free the trapped electron and emit it from the crystal. This model was proposed by Apker and Taft² to account for peaks observed in their external photoeffect spectra.

(4) Two-step ionization. The stimulation energy may promote the trapped electron to an excited state of the F-center from which it can be thermally or optically stimulated into the conduction band. Once in the conduction band the electron may acquire enough energy to escape. This process should produce a resonance-like emission centered about the absorption energies of the F-center, and the emission energy should increase with temperature.

(5) Auger-like emission. Tolpygo et al.²⁴ suggested that any one of the thermoluminescence processes shown in Figure 4 could give up its energy in the form of an emitted electron, rather than as a photon. This would be a process similar to the Auger effect of atomic physics. This model could produce an emission peak corresponding to the F-center absorption band in the case of Figure 4(D), a wide emission peak on the high energy side of the absorption band in the case of Figure 4(B), and a wide band corresponding to the untrapping of holes in the case of Figure 4(C).

Statement of Purpose

Although this experiment was largely exploratory in nature, there

were four specific motivations for it. The primary purpose was to repeat the OSEE studies of Petrescu¹³⁻¹⁶ using an improved apparatus in which simultaneous measurement of electron emission and optical absorption could be made under high vacuum conditions. This method should give definite information about the correspondence of emission and absorption peaks.

There has been some question as to whether the peaks observed by Bohun, Sujak and Petrescu were produced by surface effects caused by the gas flow counting technique. Sujak pointed out that early experiments performed in vacuum did not produce these emission peaks.²⁵ The technique employed here should eliminate this problem.

Since all of Petrescu's data were obtained from thin polycrystalline layers of salts evaporated or melted onto a substrate, it was of interest to discover whether the same OSEE spectrum would be obtained from a monocrystal as from a polycrystalline layer.

In the case of potassium chloride Petrescu observed peaks corresponding to the F-center absorption and to the M-center band in the infrared.¹⁴ He did not, however, investigate the region on the high energy side of the F-band. Potassium chloride is a particularly suitable material for studying the K and L transitions which occur in this region because the F-band lies in the middle of the visible region at 540 nm. Therefore in this experiment particular attention was given to the region of the spectrum between 300 and 650 nm.

The procedure of this experiment was to irradiate a potassium chloride single crystal with 3 keV electrons and to measure simultaneously the optical absorption and the exoelectron emission spectra of the damaged crystal. These spectra were studied as a function of accumulated

radiation dose, crystal temperature, external magnetic field strength, direction of monochromator scan, and light exposure time.

CHAPTER II

APPARATUS

Vacuum System

The experiments described here were carried out in the high vacuum region of 10^{-6} torr. Pumping was accomplished by the successive use of two cryogenic sorption pumps and a titanium sublimator. The bell jar of the system was constructed of 303 stainless steel by the Oklahoma University machine shop. All components of the experiment were housed within this bell jar, and it was sealed to the vacuum chamber by a Viton gasket to allow easy and rapid cycling of the system between vacuum and atmospheric pressure. All other vacuum seals were formed by metal gaskets. A vapor trap of alumina pellets was installed between the mechanical pump and the sample chamber to insure that oil vapor could not enter the system.

The normal operating procedure was to operate: (1) the mechanical pump to a pressure of 10^{-3} torr, (2) the cryopump to 10^{-5} torr, and (3) the sublimation pump to 10^{-6} torr. The cryopump was sufficient to maintain the system at 10^{-6} torr during the experiment.

Sample Holder

The sample holder, shown in Figure 5, consists of a 45° right circular cone of stainless steel having two perpendicular planar surfaces

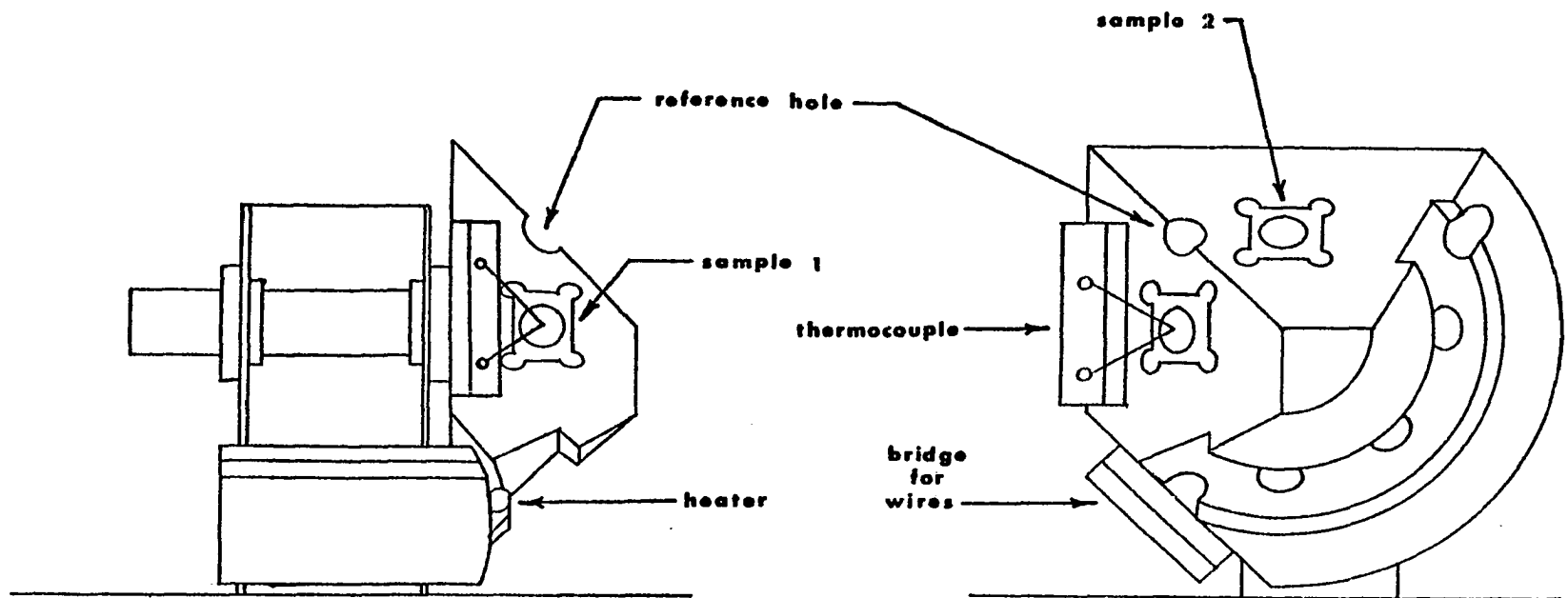


Figure 5. Sample holder.

milled into its face. These planar surfaces serve to support two samples. Three 1/4-inch diameter holes were drilled perpendicular to the axis of the cone and 45° apart. The two mutually perpendicular holes function to admit light from the monochromator to the rear surface of each crystal, while the third hole allows light to pass unobstructed to the photomultiplier in order to measure a reference light intensity curve. This configuration is shown schematically in Figure 6.

The conical holder also contains a 135 watt cylindrical immersion heater and a terminal block of MACOR glass ceramic which supports two chromel-alumel thermocouples. One thermocouple is clamped between the terminal block and the sample holder near the heater. It is used to provide a signal for the temperature control circuit (see Appendix 6). The second thermocouple presses against the exposed surface of one crystal providing a measurement of the actual surface temperature of that sample.

The sample holder is mounted on two 0.030 inch thick stainless steel bearings by means of bronze bushings in order to minimize heat loss. It can be rotated by means of a Varian rotary motion feed through. A detent system outside the vacuum chamber allows the sample holder to be accurately positioned at 45° intervals about its axis. The thermocouple and heater wires are insulated with glass beads and held in a flat cable configuration by MACOR spacers. This cable is coiled tightly around the axle so that it can wind and unwind as the sample holder rotates.

Electron Gun

The base plate of the sample holder supports an electron gun used to irradiate the crystal as shown in Figure 6. The electron gun is

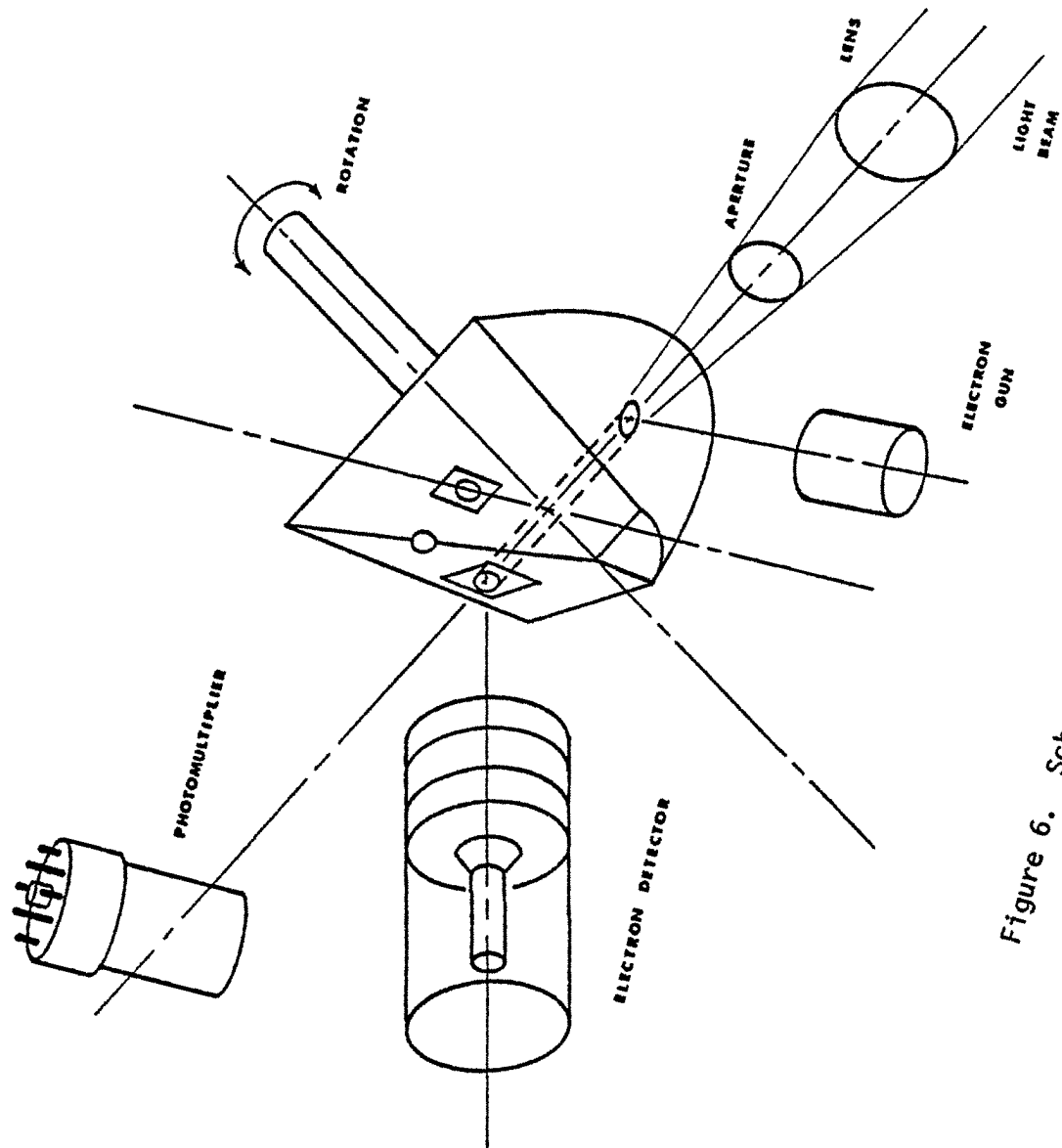


Figure 6. Schematic of experiment.

located on the same side of the sample holder as the entrance optics for the light beam. The beam from the gun makes a 45° angle with the light beam thus striking the surface of the crystal perpendicularly, i.e. along the (100) planes of the crystal lattice. The sample holder is first rotated so that the crystal faces the electron gun during irradiation, and then it is rotated 180° to face the electron detector for readout.

This electron gun consists of a Pierce element²⁷ and a pair of deflection plates producing a beam of 3° divergence angle which has a 1 cm diameter at the crystal surface. Beam currents of 300 μ a at 3 keV have been produced. The cathode of the gun consists of a 1/16 inch diameter tantalum disk 0.002 inches thick, spot-welded onto a loop of tungsten wire. Although a voltage drop of about 5 volts exists across the filament wire, the electrons emitted from the tantalum disk are monoenergetic (except for the Maxwell distribution) because the disk touches the filament at only one point. This type of cathode is advantageous because it can be cycled between vacuum and atmospheric pressure many times without degrading its emission properties.

A 60% transparent copper wire mesh was placed in the electron beam path between the gun and the sample holder. Current intercepted by this mesh was calibrated against the current from a Faraday cup placed at the irradiation position of the sample holder. In this way the irradiation dose could be measured for each sample.

Electron Detector

Charged particles originating at the sample were detected by means of a channeltron electron multiplier. Signal pulses from the

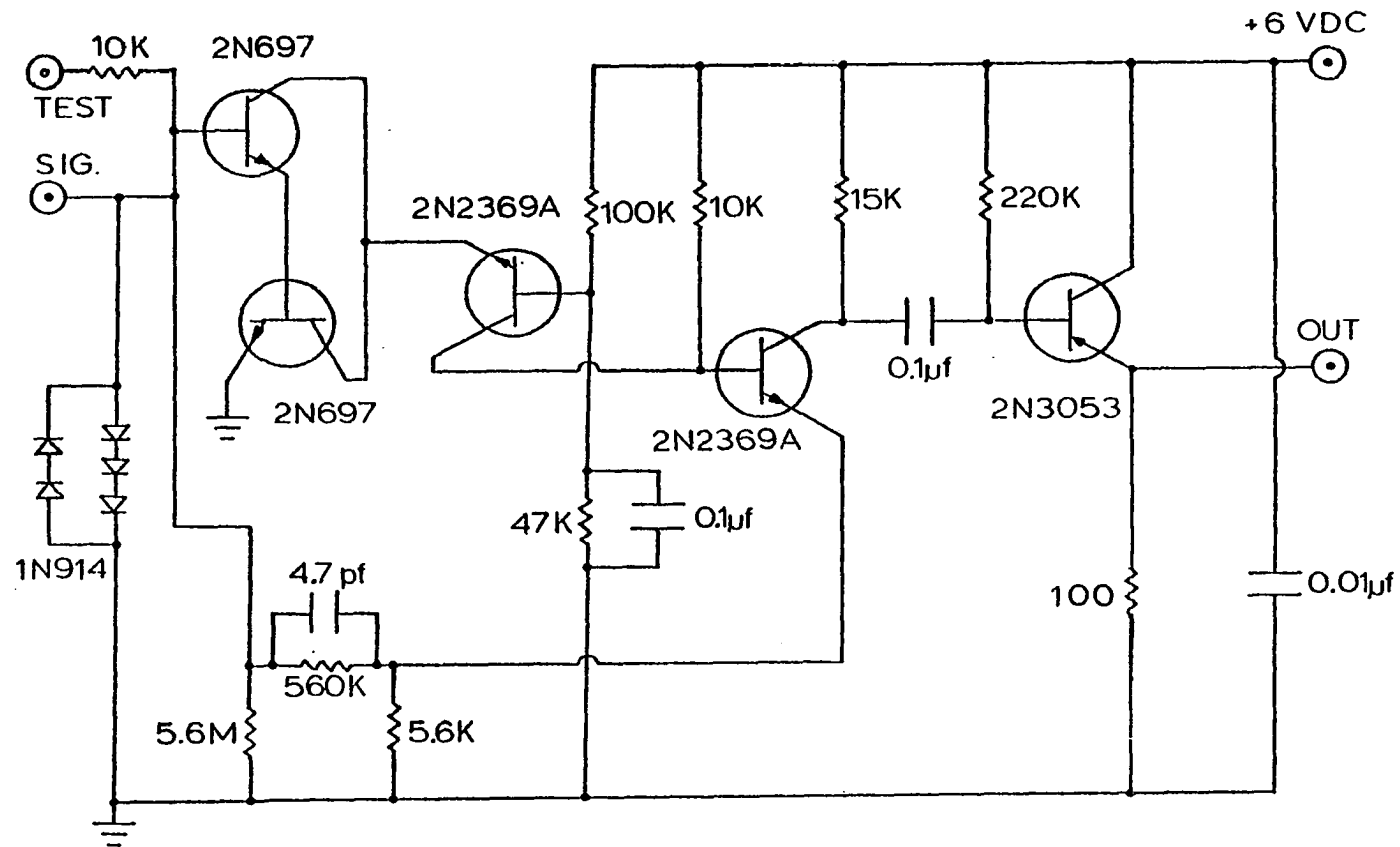


Figure 7. Charge sensitive pre-amplifier.

channeltron were coupled through an external capacitor to the input of a charge sensitive pre-amplifier (Figure 7) and then to an Ortec spectroscopy amplifier and single channel analyzer.

The channeltron has an entrance aperture of 1 cm diameter and was placed 1 cm away from the crystal. The exposed surface of the crystal was also 1 cm diameter giving a solid angle of about 1.5 steradians. The channeltron was sufficiently far from the crystal to allow the light beam shining through the crystal to pass undisturbed to the photomultiplier tube.

Optical System

For alignment and initial checkout the light source used was a standard 500 watt CZX projector lamp. The data presented in this paper were obtained using a 150 watt xenon discharge lamp with regulated power supply and f/1.0 quartz optics.

Light from the lamp passed through a Spectrolab f/1.0 grating monochromator before entering the vacuum chamber. The input and output optics of the monochromator consist of 3-1/2 inch diameter quartz lenses and a front surface plane mirror coated with aluminum. The entrance and exit slits are continuously variable from 0.01 to 4 millimeters with a dispersion of 7.6 nm/mm. Order sorting filters were used in the output optics to eliminate the light from second order spectra.

The monochromator scan is continuous and motor driven. Its speed can be selected at 0.05, 0.1, 0.2, 0.5, 1.0, 2.0, 5.0, 10.0 nanometers/second. The wavelength dial has been modified to allow a light beam to trigger a phototransistor at 1 nanometer intervals thus providing

channel advance pulses to the multichannel analyzers. The motor drive can be started or stopped remotely by a TTL controlled relay.

An image of the monochromator's exit slit is formed 6.5 centimeters from its output lens, thus necessitating another lens in order to focus this image onto the rear of the crystal 24 centimeters away. Light enters the vacuum chamber through a one-inch diameter quartz window and passes through a one-inch diameter plano-convex lens as in Figure 6. A limiting aperture is placed between the plano-convex lens and the sample holder to minimize reflections as the beam passes through the sample holder.

Unlike the earlier experiments¹⁰⁻¹⁶ the light beam enters the crystal from its rear surface and passes through the crystal before producing exoelectron emission. This configuration has the advantage of allowing optical absorption to be measured simultaneously with exoemission. This is justified by the fact that exoemission effects are known to take place within 10^{-6} cm of the exposed surface,⁴ and that a 5 keV electron beam should produce coloration only to a depth of about 10^{-7} cm in KCl.²⁶

Light passing through the crystal can leave the vacuum chamber through a second quartz window, and is detected by a Hamamatsu R928 photomultiplier tube. This tube has a response range of 185 to 930 nm.

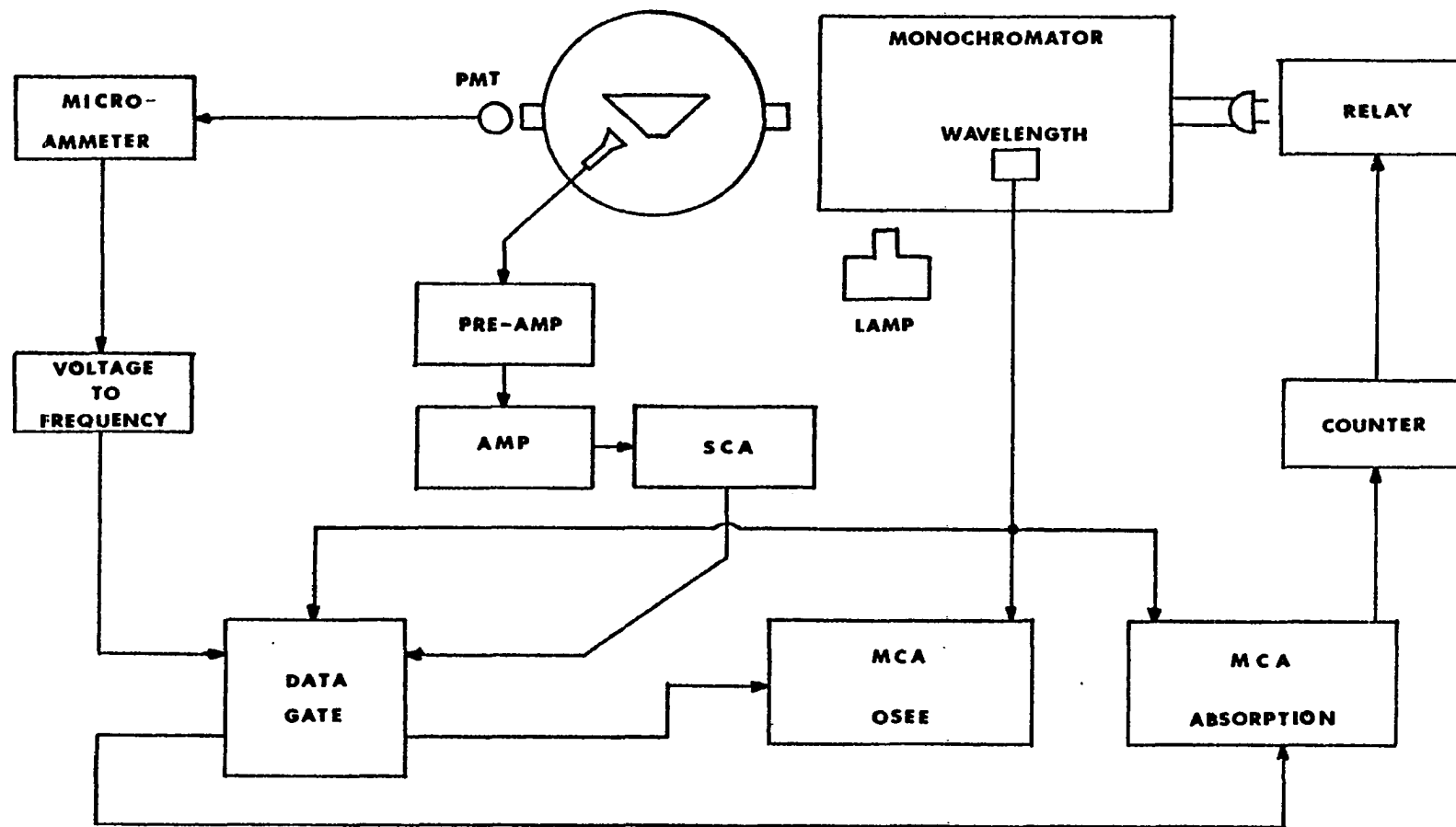


Figure 8. Block diagram of electronics.

CHAPTER III

DATA COLLECTION METHOD

The data to be recorded in this experiment were the intensity of light transmitted through the sample and, simultaneously, the intensity of electron emission from the sample surface. Both these intensities were to be recorded as a function of wavelength of the external light source. Two Ortec multichannel analyzers (MCA) were used to assemble the spectra. These analyzers were operated in the multiscale mode with channel advance pulses being supplied by a phototransistor circuit which was added to the Spectrolab monochromator. A channel advance pulse was generated every nanometer during the scan and the time base switches of the MCA's were set to divide by two so that each channel represented a wavelength change of 2 nanometers.

In this mode of operation the multichannel analyzers are "slaved" to the monochromator and so they follow along with its scan regardless of the speed. Channel advance pulses are generated only while the scan motor is running so the MCA's can be placed into their RUN mode at any time; they will only begin accumulating data after the monochromator is started. Power to the scan motor is controlled by the TTL relay circuit of Appendix 4. This relay is energized by a gate signal from a presetable

up/down counter--see Appendix 1--which counts the channel advance pulses, and therefore controls the length of the scan.

In normal operation the up/down counter is set to count down from 177 to zero. The MCA's are placed in their RUN mode and the counter is started. Starting the counter energizes the relay and starts the scan motor. Channel advance pulses begin to flow to the MCA's which begin to input and store their respective data, and the counter keeps track of the accumulated channels until 177 channels have been counted. At that point the counter releases the relay and the monochromator stops. This scheme is shown in Figure 8.

The OSEE spectra are assembled by counting pulses from the channeltron into one of the MCA's. These pulses are amplified by a factor of 10^3 by the combination of a charge-sensitive pre-amp and an Ortec model 471 spectroscopy amplifier. They then go to a single channel analyzer where noise can be discriminated out before being counted in the MCA.

Optical absorption data are collected by a two step process. First a reference spectrum is taken of intensity versus wavelength for light passing unobstructed through the hole in the sample holder. Then the intensity of light transmitted through the crystal is recorded. A Hamamatsu R928 phototube is used to detect the light and its output current is measured by a Keithley 610C multimeter. In order to record this signal in the MCA the output of the Keithley meter is converted to a pulse train whose frequency varies linearly with the current from the phototube. The voltage controlled oscillator (VCO) circuit used to accomplish this conversion is described in Appendix 2.

Because the MCA's are connected as slaves to the monochromator a problem arises if the channel advance pulses from the monochromator are not equally spaced in time. Each channel in the MCA accumulates data until the next channel advance pulse is received. Thus the channels represent not only wavelength but also time. If the advance pulses are not equally spaced then some channels will collect data longer than others and the accumulated spectrum will be distorted. The advance pulses are generated by a phototransistor which is activated by a light beam passing through holes drilled in the wavelength dial of the monochromator. Not only is it difficult to evenly space the holes on the dial, but also the light intensity may fluctuate due to reflections from the walls of the moving holes.

To minimize this problem both the electron signal and the light intensity signal are passed through a monostable gate circuit (Appendix 3). When a channel advance pulse arrives from the monochromator the gate circuit is enabled and data pulses begin to pass to the MCA's. The length of time the gate remains open depends upon an RC time constant which is set to have the same duration as the minimum time interval between successive advance pulses. In this way data passes to the MCA's for the same length of time between each two advance pulses, and any data coming after the gate closes are ignored.

A normal spectral scan of a crystal consists of four data sets each containing 177 values corresponding to 177 different wavelength values at 2 nanometer intervals between 300 and 652 nanometers. Two of the data sets record the intensity of exoelectron emission. One of these is a background emission spectrum taken by shining light through

the hole in the sample holder, and the other is the emission spectrum of the sample. The other two data sets represent light intensity passing through the hole and through the crystal. After these four spectra are accumulated in the MCA's, the values are transferred digitally at a rate of 2400 BAUD to a Tektronix 4051 minicomputer where they are recorded on magnetic tape and processed for plotting. The data processing algorithms consist of a routine for calculating the extinction coefficient for the sample and a routine to adjust the electron spectrum for relative light intensity.

The extinction coefficient is defined as:

$$D = \text{LOG}\left[\frac{I_0}{I_t}\right]$$

where I_0 is the incident light intensity and I_t is the intensity transmitted through the sample. Since the sample intercepts the light beam at 45° an appreciable fraction of the incident light is reflected from the crystal surfaces. This reflected light will produce a non-zero value for D even when the crystal is uncolored. This base line shift is compensated by subtracting from D a value D_0 which is the extinction of the freshly cleaved sample before exposure to any radiation. The extinction coefficient has been used for this experiment rather than the optical absorption coefficient because it was not possible to determine the exact thickness of the colored layer produced at the crystal surface.

Petrescu reported that he did not correct his OSEE data to account for the spectral shape of the stimulating light.¹³ He noted that the count rate of detected electrons was so low that the lineshapes were

probably limited by the number of emission centers rather than the intensity of the light. In the present experiment, however, normal exoemission rates were 10^2 to 10^3 electrons per second, and the characteristic emission lines of the xenon lamp were clearly reflected in the raw exoemission data. It was therefore necessary to normalize the spectra with respect to light intensity. Since both light intensity and exoemission are recorded simultaneously this would merely require a point-by-point division of the two data sets except for the fact that the recorded lamp spectrum has been convoluted by the response characteristics of the photomultiplier tube. Therefore the lamp spectrum must be corrected for the phototube response before it is used to normalize the exoemission spectrum. A typical lamp spectrum as detected by the phototube is shown in Figure 9. The photomultiplier response curve was obtained by recording a lamp spectrum taken first with the phototube and second with a thermopile. Based upon the assumption that the thermopile has constant response independent of wavelength, dividing these two spectra yields the phototube response shown in Figure 10.

Irradiations of the samples were performed using a 3 keV accelerating potential on the electron gun. The Keithley 610C picoammeter was connected to the electron beam grid to monitor irradiation current. The output of the picoammeter remained connected to the VCO. Accurate dose control was obtained by counting the output pulses of the VCO to determine the irradiation time. Since the frequency of the VCO depends linearly upon the beam current, then the number of pulses counted during irradiation is proportional to the product of the beam current and the irradiation time, which is itself proportional to energy

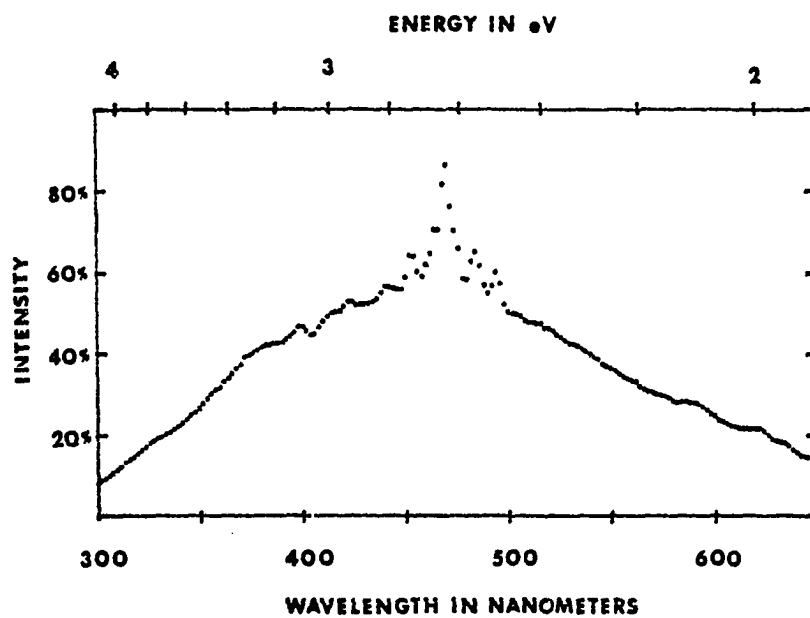


Figure 9. Emission spectrum of xenon lamp.

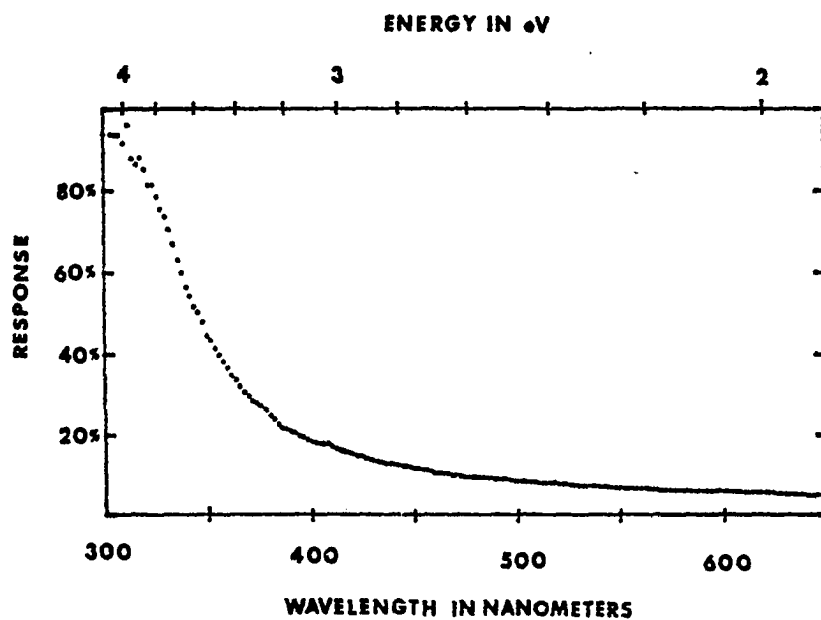


Figure 10. Response of photomultiplier.

deposited. Typical irradiations were 10 μa for 10 seconds which amounts to 0.3 joules deposited on an area of 0.78 cm^2 . The surface temperature of the crystal was observed to rise about 6°C on the average during this irradiation.

CHAPTER IV

RESULTS

A typical series of spectra taken on a freshly cleaved KCl single crystal are displayed in Figure 11. Curves designated by capital letters represent OSEE spectra and curves labelled with lower case letters are the corresponding optical extinction spectra. Figure 11(A) is a spectrum of the freshly cleaved unirradiated crystal at 26°C. Some emission is observed above about 2.8 eV. The optical absorption of the new crystal is taken to be zero and used as a baseline for all succeeding runs.

After exposing the crystal to white light from a 175 watt projector lamp for 30 minutes the exoemission becomes undetectable when displayed on the same scale; see Figure 11(B). The bleached crystal displays a slight increase in optical absorption, but this increase is of about the same magnitude as the error expected from instabilities in lamp intensity and sample holder positioning (± 0.02 in units of extinction coefficient).

The new crystal was irradiated for 10 seconds with a 3 keV electron beam at 20 μ a beam current causing the surface temperature of the crystal to rise to 38°C. No temperature change was detectable on the sample holder. The spectrum shown in Figure 11(C) was run 13

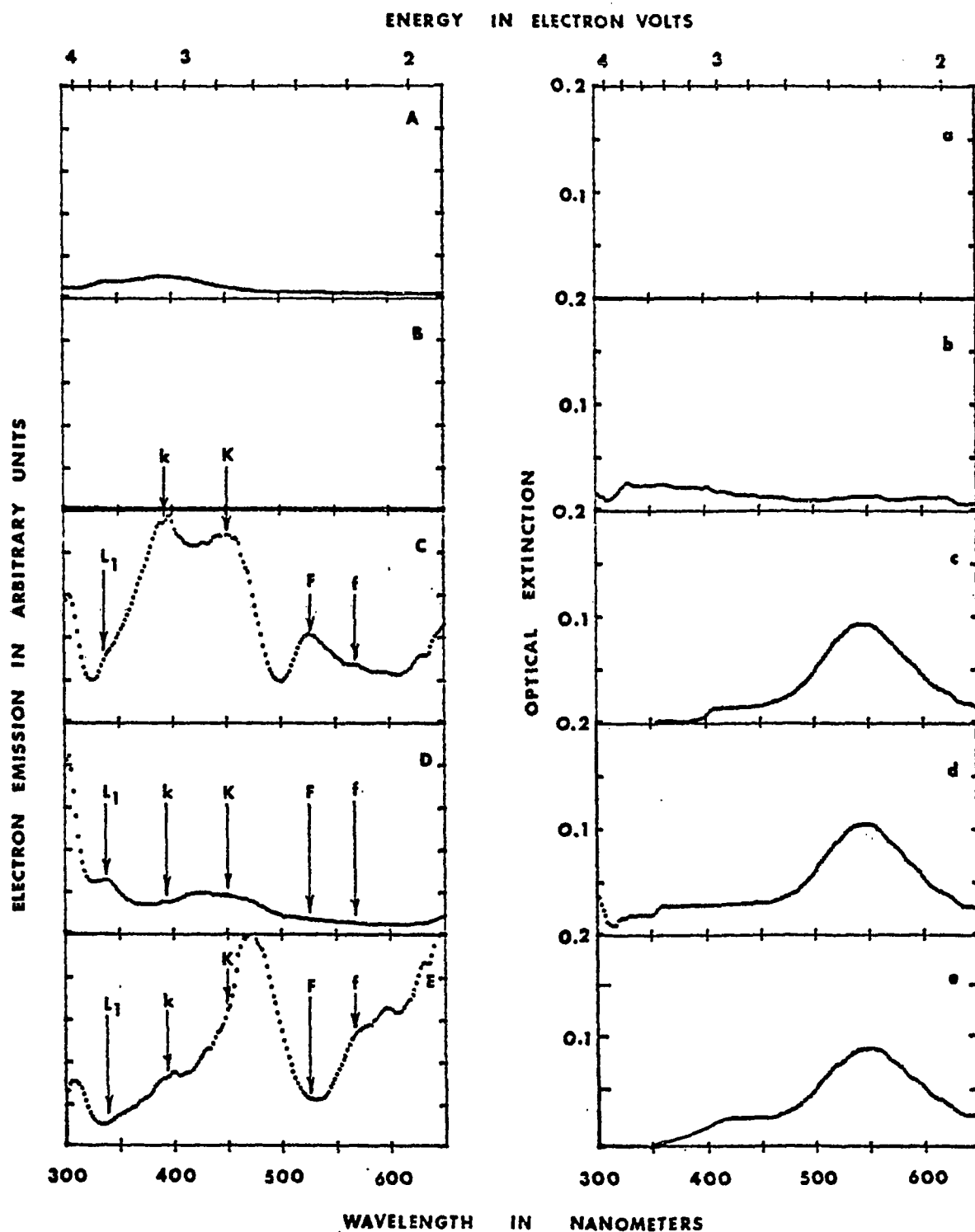


Figure 11. Exoemission spectrum (capital letters) of KCl single crystal and simultaneous optical extinction spectrum (small letters). (A) new crystal, (B) 30 min. white light bleach, (C) 3 keV e^- irradiation, (D) second scan after irradiation, (E) after sitting for 24 hours.

minutes after irradiation when the surface of the crystal had cooled to 28°C. A typical F-center absorption band was detected at 540 nm with some structure appearing on the high energy side corresponding to the weaker K-band.

The OSEE spectrum of the irradiated crystal displays a peak at 526 nm corresponding to the high energy side of the F-center absorption band. Note that the F-absorption band is centered at 540 nm and is quite symmetric while the emission peak is located at 526 nm and is skewed toward higher stimulation energies. All of the emission peak is contained within the area under this absorption band. The emission peak appears to have a shoulder on the low energy side at 570 nm, labelled f in Figure 11. The F-emission band corresponds well in overall shape with that reported by Petrescu.¹⁴ In addition three overlapping peaks appear to the high energy side of the F-band at 340, 395, and 450 nm. The peaks at 340 nm and at 450 nm correspond well with published values for the optical absorption of the L_1 -band at 344 nm and the K-band at 459 nm.¹⁷ The most prominent feature located at 395 nm has been observed in photoconductivity measurements,³⁴ but does not appear to correspond to any well known absorption band. This peak is labelled k in Figure 11.

Petrescu made no attempt to identify the double peak appearance of the exoemission from the F-band. It is known that the F-absorption band splits into two peaks when impurity alkali atoms exist substitutionally at lattice sites next to the F-center. While the crystals used in this experiment were grown from "pure" salts a certain amount of impurity atoms are to be expected, and the double emission peaks at 526

and 570 nm correspond well with the published absorption peaks for KCl(Na) of 527 and 585 nm.²¹ The fact that this splitting does not appear in the measured extinction spectrum is probably due in part to the width of the extinction peak and partly to the very weak coloration of the crystal.

Figure 11(D) shows a second spectral scan of the crystal taken six minutes after the first scan. While the optical absorption spectrum has changed very little from the first run, the exoemission has been substantially bleached away by the light exposure of the first scan. The L_1 -band at 340 nm has bleached much less than all the others.

The crystal was left undisturbed for 24 hours at room temperature and a spectrum was again taken without further exposure to radiation. Figure 11(E) shows that the OSEE has again increased in intensity. It is interesting to note that a minimum in the emission curve occurs near 540 nm where the F-center maximum occurred previously. Petrescu noted this kind of behavior and attributed it to an inversion of peaks caused by an emission intensity large enough to become space charge limited.¹⁴ This explanation is difficult to understand based upon the current experiment since the Child-Langmuir space charge law would demand electron energies of less than about 10^{-7} eV before emission currents would be limited to less than 1000 counts/sec.²⁷ The entire spectrum is markedly different and suggests that the surface condition of the crystal plays an important role in the position and intensity of the exoemission peaks.

The exoemission spectrum of this KCl single crystal is compared with that of a polycrystalline layer of analytical reagent grade KCl

salt in Figure 12. The polycrystalline layer of Figure 12(A) yields an exoemission spectrum about four times more intense than that of the single crystal (note scale change), probably due to the increased surface area. The two spectra are very similar in shape with the exception that the L_1 peak is much more intense in the polycrystalline sample. It is clear that the use of polycrystalline samples by the early investigators is justified and in fact produces a somewhat stronger signal. However, it is very difficult to measure the optical absorption of a polycrystalline layer because of the large amount of scattered light. This makes it necessary to rely upon absorption data taken with single crystal samples in order to identify the exoemission peaks.

Since exoemission phenomena have been considered for many years as a possible dosimetry technique, the OSEE spectra were studied as a function of energy deposited in the crystal. Each crystal was irradiated and scanned several times in succession, and the results are plotted as a function of cumulative exposure in Figures 13 and 14. It is clear from these plots that the OSEE peaks between 300 and 650 nm decrease in intensity with increasing irradiation doseage--just opposite from the behavior desired for dosimetric applications. Moreover the shape of the exoemission spectrum seems to change dramatically with increasing exposure. Emission in the F-band disappears after a few exposures leaving only weak K and L_1 -bands. In the case of the second sample (Figure 14) where the double peak character of the F-band is prominent, it appears that the longer wavelength F-peak disappears first, followed by the higher energy peak two doses later. Besides having different spectral shapes, the two crystals differ in the rate at which their

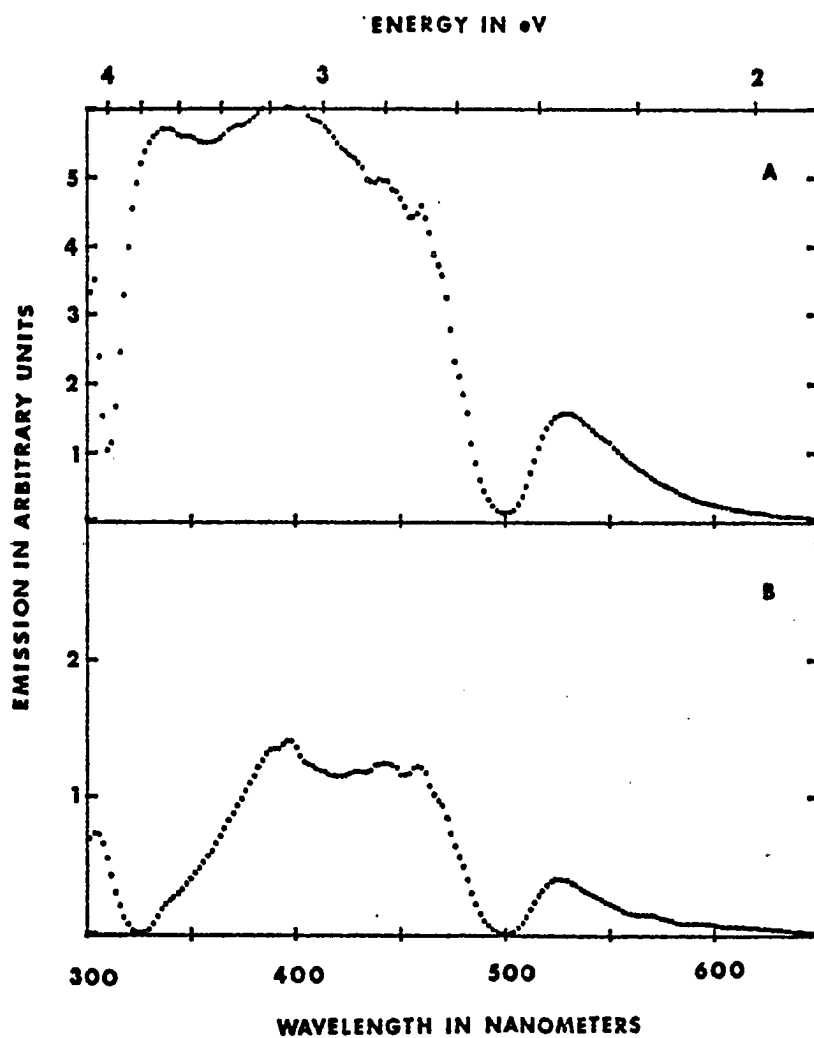


Figure 12. Exoemission from: (A) polycrystalline sample, (B) single crystal.

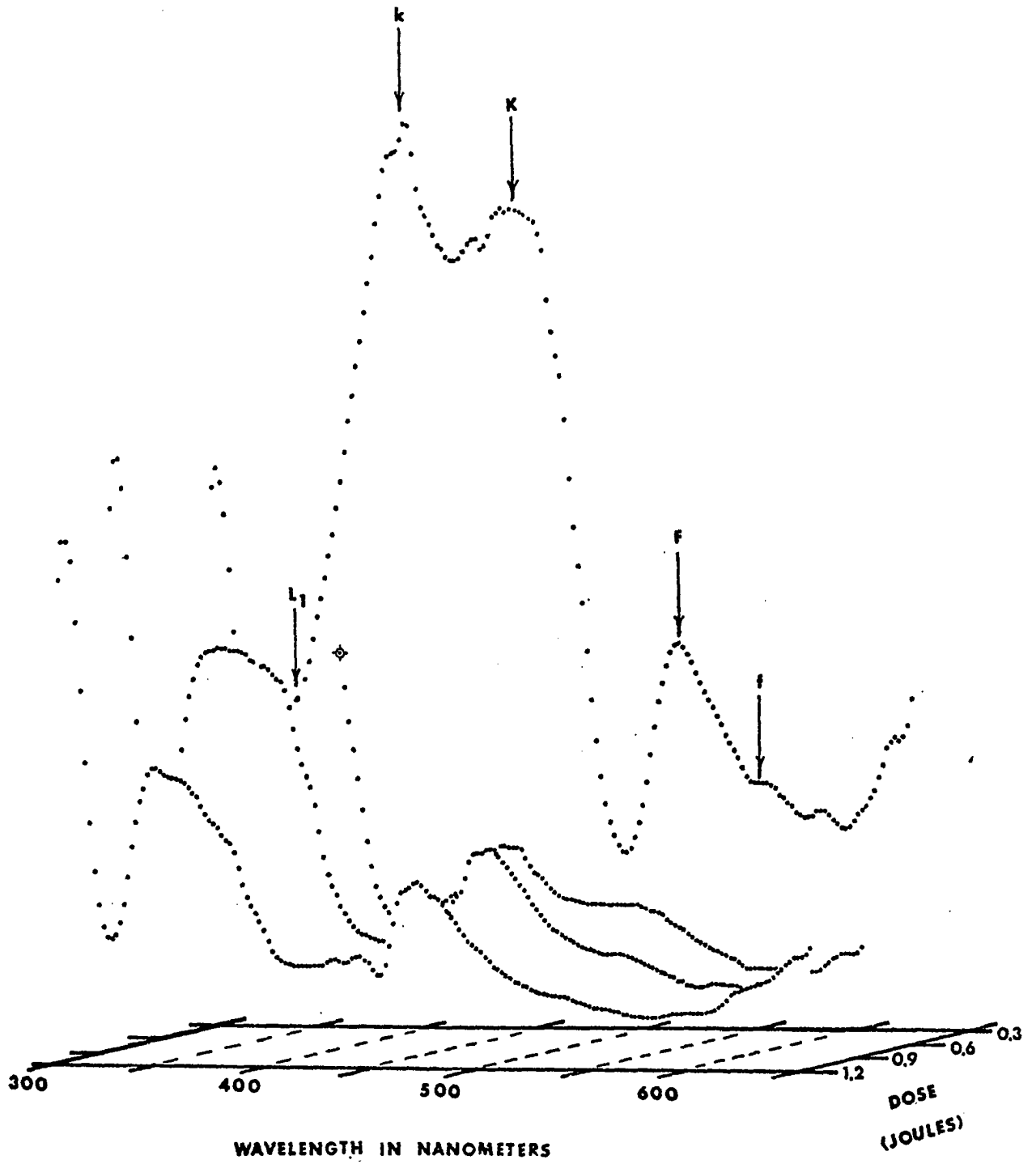


Figure 13. Exoemission spectrum versus cumulative dose for KCl single crystal number 1.

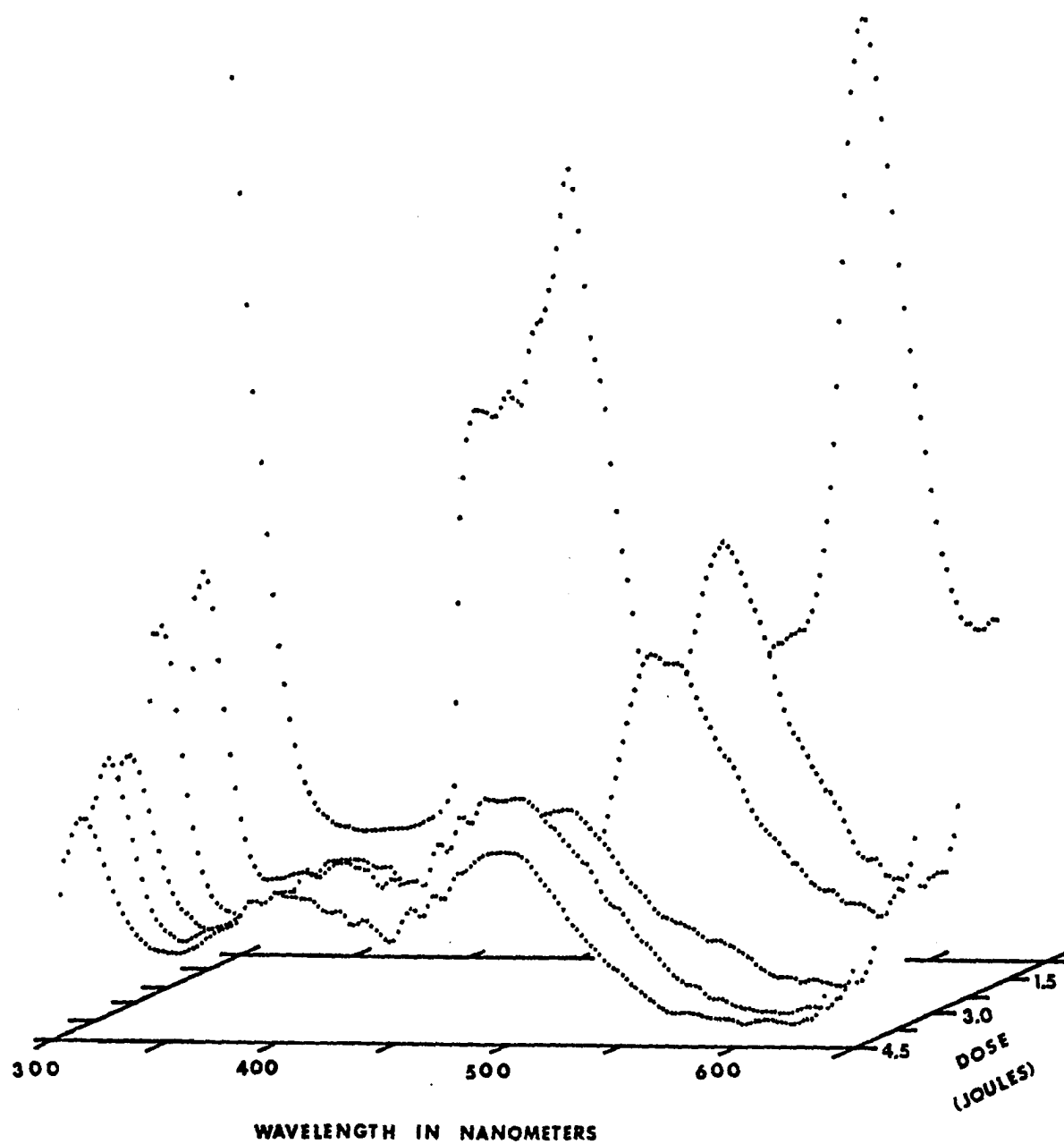


Figure 14. Exoemission spectrum versus cumulative dose for KCl single crystal number 2.

F-bands are destroyed by successive irradiations. Only 1.2 joules were necessary to eliminate the F-band in the first crystal while it is just visible in the second crystal after 3 joules.

Soul and Tubbs have shown that under successive irradiations by low energy (5 keV) electron beams the F absorption band in KCl does not continually grow in intensity but reaches a peak value at an extinction coefficient of about 0.2 and then falls to a lower equilibrium value corresponding to an F-center concentration of about 0.3% of the available lattice sites.²⁶ The same behavior was observed in the absorption curves measured in this experiment.

It should be pointed out that, while it has been established for several years that thermally stimulated exoemission yield does increase linearly with dose, those experiments were performed using x-ray irradiation or high energy electron beams where the penetration depth is of the order of the sample thickness (see Becker⁴). Also in the present experiment no attempt was made to compare the integrated electron emission for the entire spectrum with the irradiation dose. The most intense OSEE occurs in the ultraviolet at energies higher than about 4 eV. This is the region of the external photoeffect of Apker and Taft, and was not investigated in the present work.

In interpreting any exoemission data it is essential to keep in mind that the surface of the sample is severely damaged by the irradiation. Not only does charging of the surface occur, but also sputtering of halogen ions is known to be a very efficient process for electron beams with energies as low as a few hundred electron volts.²⁸ In fact Palmberg and Rhodin have shown that irradiating KCl with a

1 keV electron beam at room temperature for several minutes produces a surface layer made up almost entirely of potassium.²⁹ This fact would seem to account for the upper limit on F-center production observed by Soul and Tubbs and is probably responsible for the decrease in exoemission intensity observed in Figures 13 and 14.

Since Soul and Tubbs²⁶ have shown the F-center concentration to remain essentially constant under repeated irradiation, we can conclude from Palmberg and Rhodin's data²⁹ that repeated irradiations must alter the work function of the crystal. We may expect the escape of low energy exoelectrons to become less likely as the surface damage increases. From Figures 13 and 14 this may imply that electrons emitted in the F-band have less energy than those emitted in the K and L bands. This view is consistent with the model of Mott and Gurney that the K and L-bands are due to electronic transitions to higher excited states of the F-center.³⁰ It also accounts for the fact that the F absorption band remains nearly constant for increasing doseage while the exoemission vanishes. Moreover Petrescu noted that in several alkali halides including KCl, the intensity of the F emission peak was enhanced by increasing the temperature by about 20°C.¹⁴ This also suggests that these electrons are more likely to escape if given additional energy.

Figures 15 through 18 display the OSEE spectrum of KCl as a function of temperature. Insets in the upper right corner show the corresponding extinction spectra. Just as in Petrescu's data the F-band emission is seen to increase with increasing temperature until 60°C was reached. A further increase to 75°C produced no change in the F-emission. At the same time that the exoemission intensity is increasing

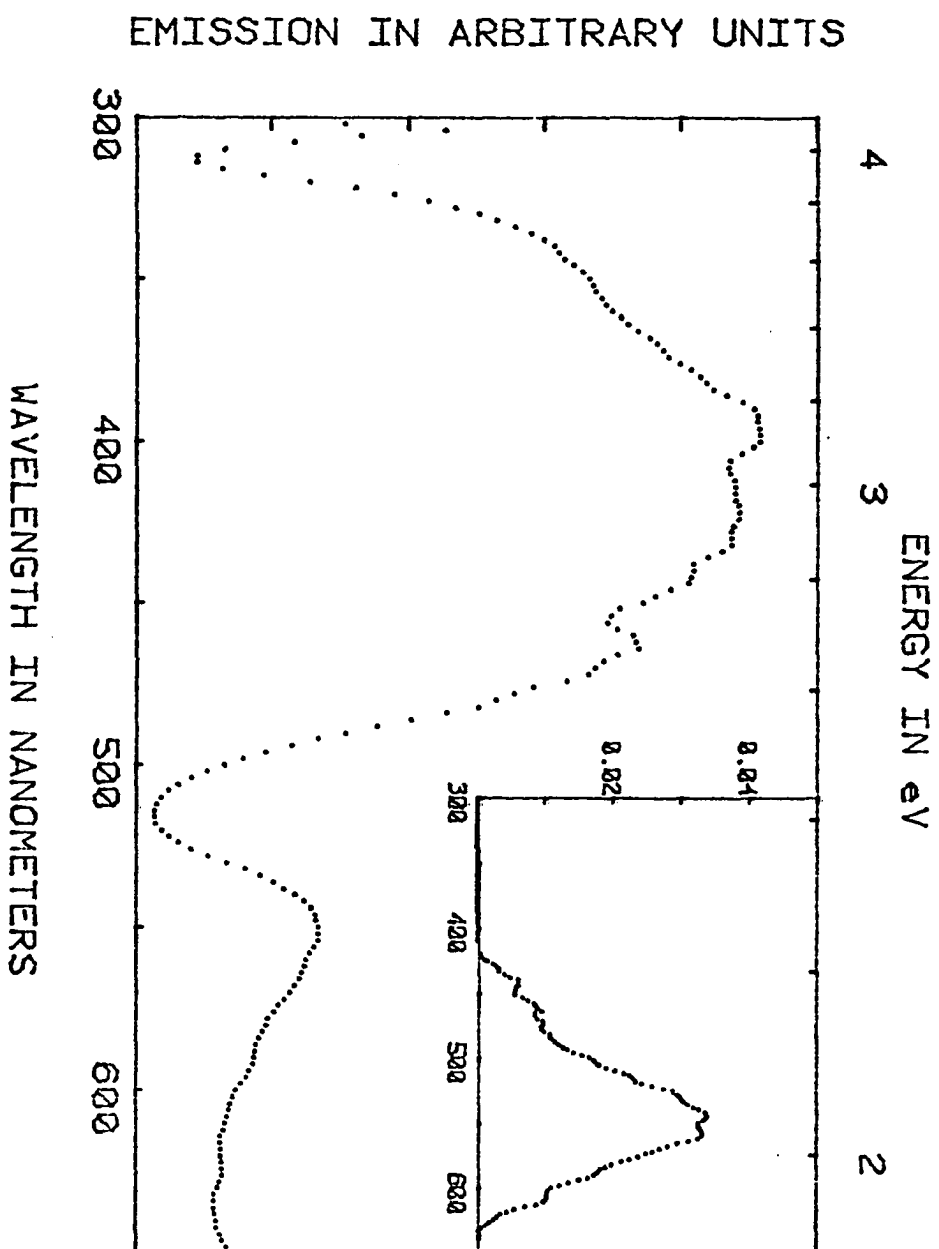


Figure 15. Exoemission of KCl single crystal at 75°C.

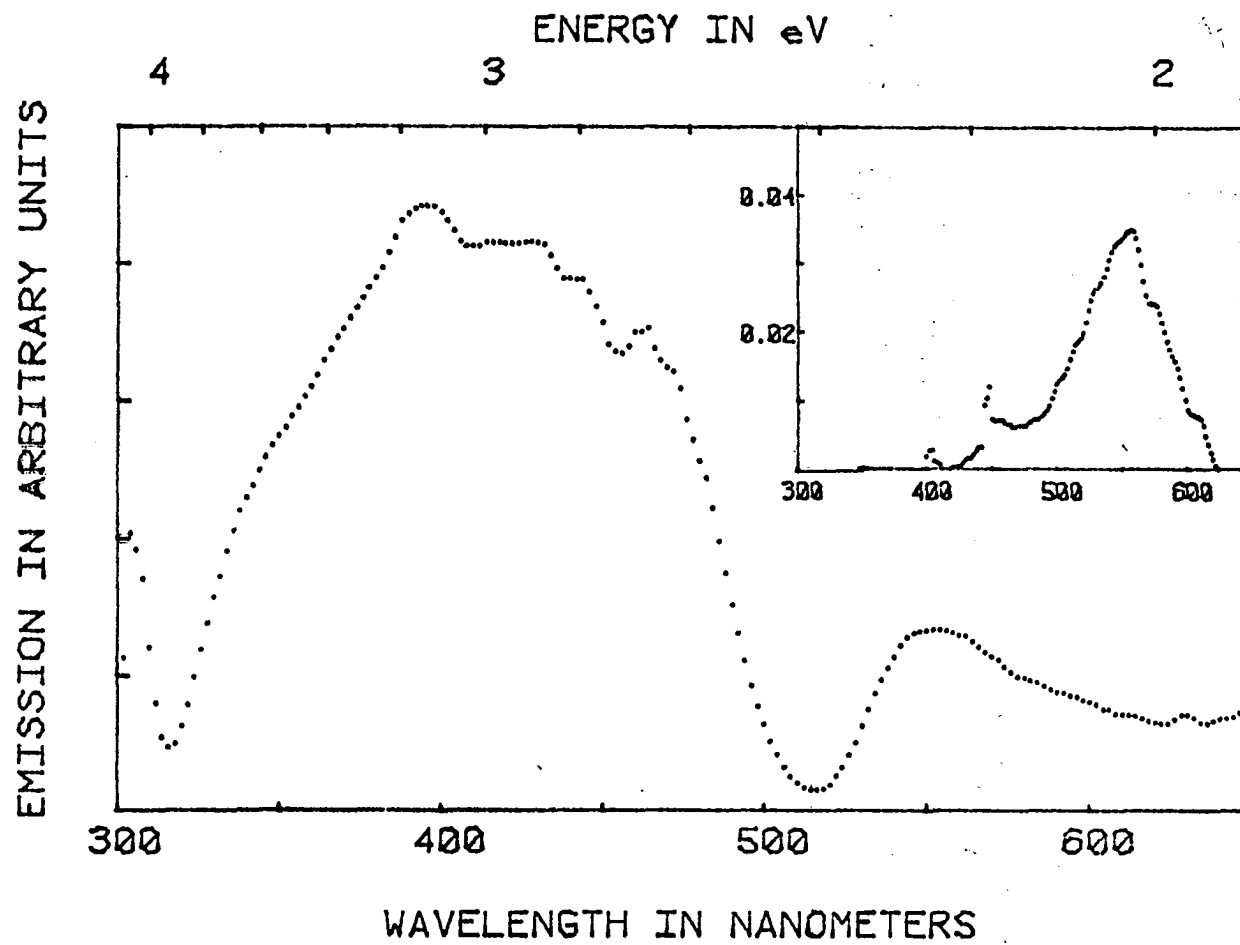


Figure 16. Exoemission of KCl single crystal at 60°C.

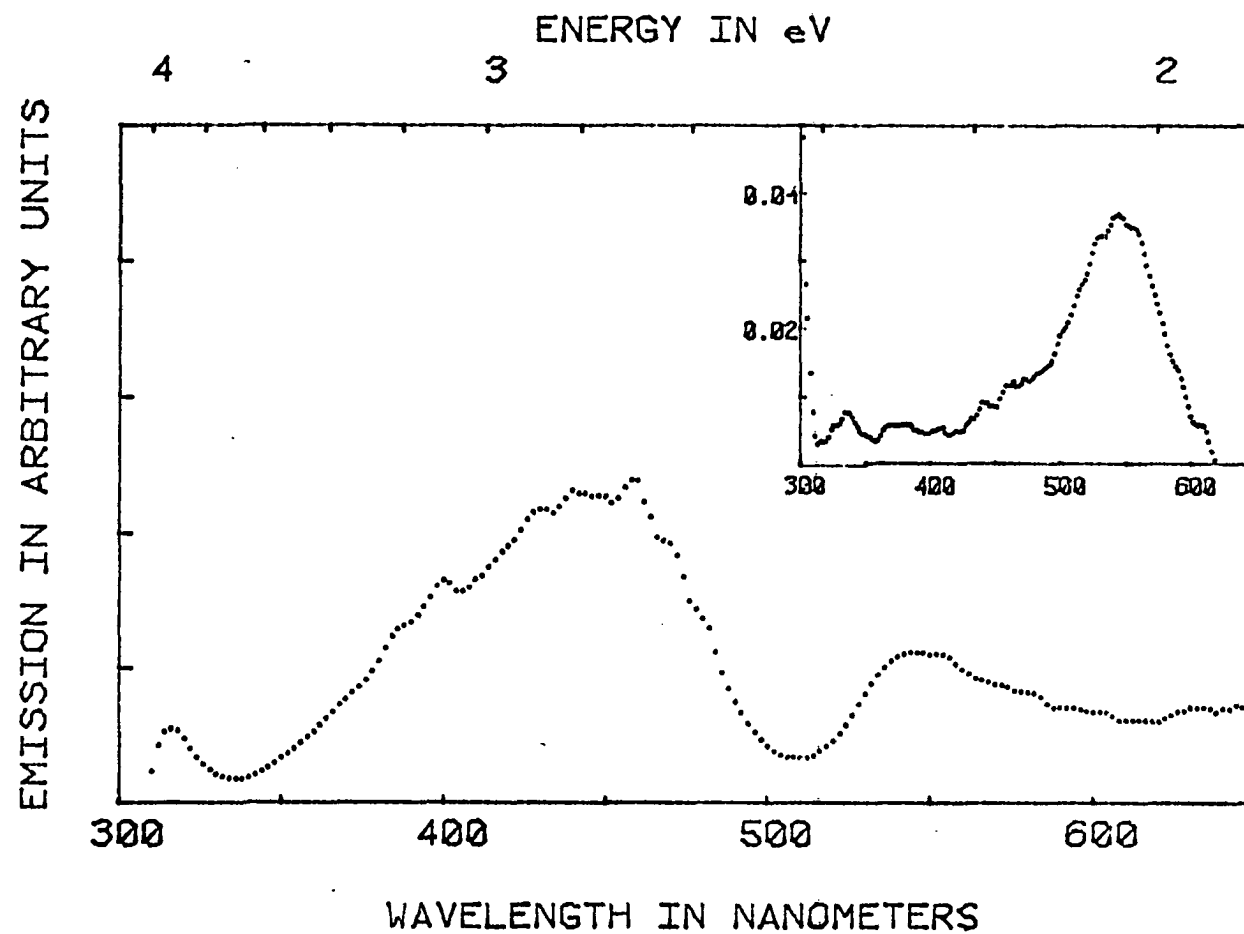
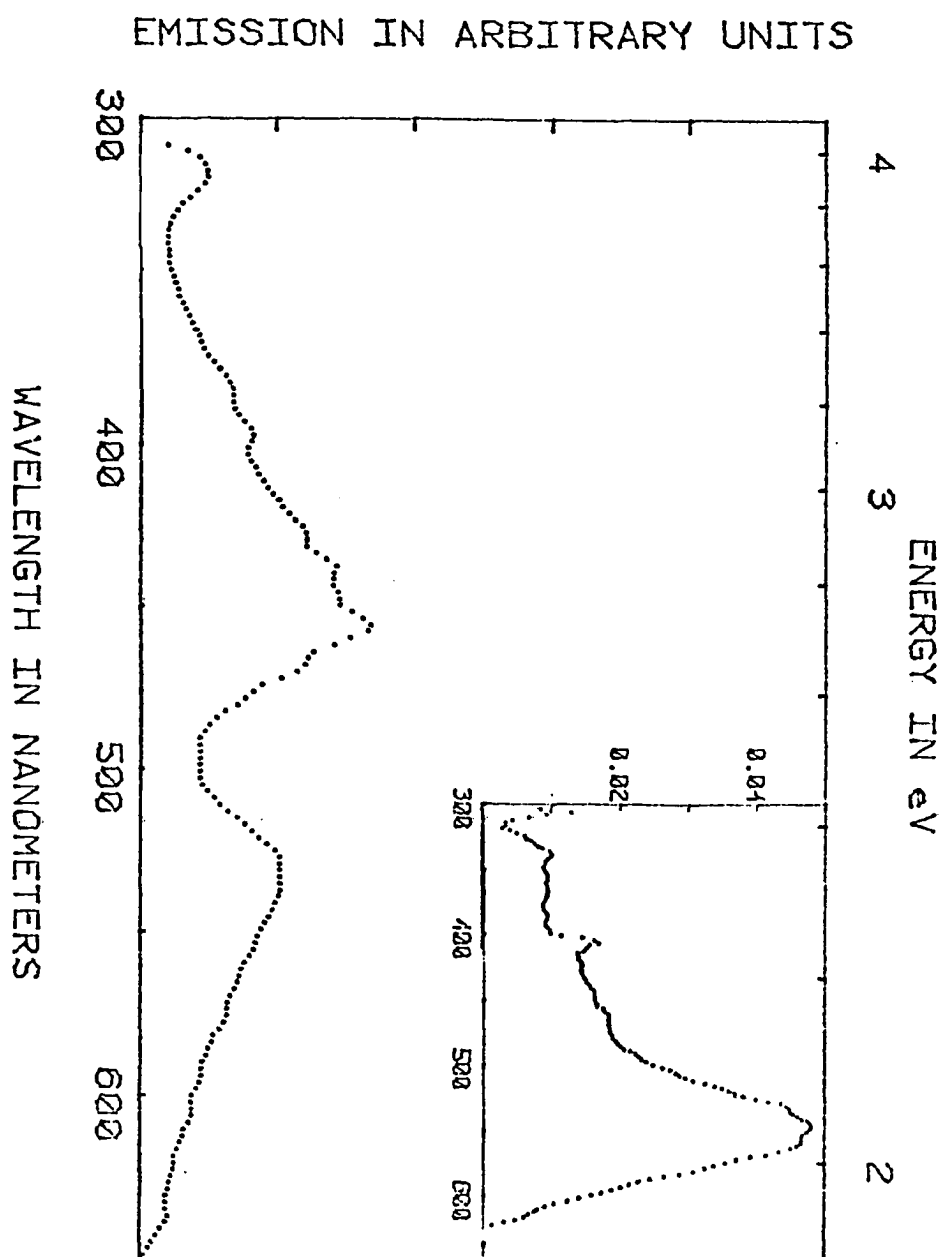


Figure 17. Exoemission of KCl single crystal at 45°C.



the F-band optical absorption is being thermally bleached away. The exoemission process must therefore account for only a small fraction of the optical absorption processes occurring at the F-center.

In addition to the increase in intensity of the F emission band, the peak also shifts to lower energy suggesting that with more thermal energy available less optical energy is needed to release the electrons. The K-band also grows with increasing temperature, but the growth of the L_1 -band and of the new band at 395 nm is most pronounced. At 30°C the L_1 -band is not detected and the 395 nm band is lost in the high energy tail of the K-band. At 60°C the 395 nm band is the most prominent feature of the curve. The L_1 -band continues to grow at 75°C after the other peaks have reached their maximum values.

To test the hypothesis that the electrons emitted from the F-band should have less kinetic energy than those emitted from the higher energy bands a crude energy discrimination scheme was tried. An external magnetic field was applied to the region between the sample and the channeltron, and the deflections of the electron trajectories were calculated. The diameter of both the sample and the detector entrance aperture was 1 cm and the distance between the two was 1 cm. For this geometry it can be shown that when a 5 gauss field is applied any electron with energy less than about 1.0 eV will be deflected more than the width of the detector aperture and so will not be counted. Likewise an 8 gauss field will discriminate against all electrons with kinetic energies below 2.5 eV. If the emitted particles happen to be ions rather than electrons the deflection of the beam should be negligible; therefore all ions will be counted.

Figure 19(A) shows the OSEE of a KCl single crystal after irradiation at 3 keV and 20 μ a for 10 sec with no external magnetic field applied. Since 5 gauss and 8 gauss magnets were readily available these two external fields were applied and the results are plotted in Figures 19(B) and 19(C) respectively. It is clear from these plots that the kinetic energy of the F and K band exoelectrons is less than 1.0 eV while many of the electrons emitted from the L_1 -band and the 395 nm band have energies lying between 1.0 and 2.5 eV. Some particles centered around the 395 nm band are detected with an 8 gauss field applied. (Note scale change in Figure 19(C).) These particles may be high energy electrons, but it seems more likely that they are photodesorbed ions similar to those detected by DeMuer and Maenhout.⁶

As an experimental check it was calculated that the 0.5 gauss field of the earth would discriminate against all electrons less than about 0.5 eV if the detector were moved to a distance of 4.2 cm from the crystal. This was done and the result is plotted in Figure 20. This suggests that the F-band electrons have less than about 0.5 eV of kinetic energy which agrees with the TSEE measurements of Gordan and Scharmann.⁷ The fact that the earth's field is sufficient to discriminate against these low energy electrons may account for the fact that they were not detected by the early experimenters working in vacuum.²⁵

Exposing a colored crystal to F-band light is known to produce new absorption bands on the long wavelength side of the F-band. These arise from aggregates of halogen vacancies known as R, M and N centers.²¹ In addition the K absorption band becomes more prominent after exposure to F-light.³¹ This means that the act of measuring the absorption spec-

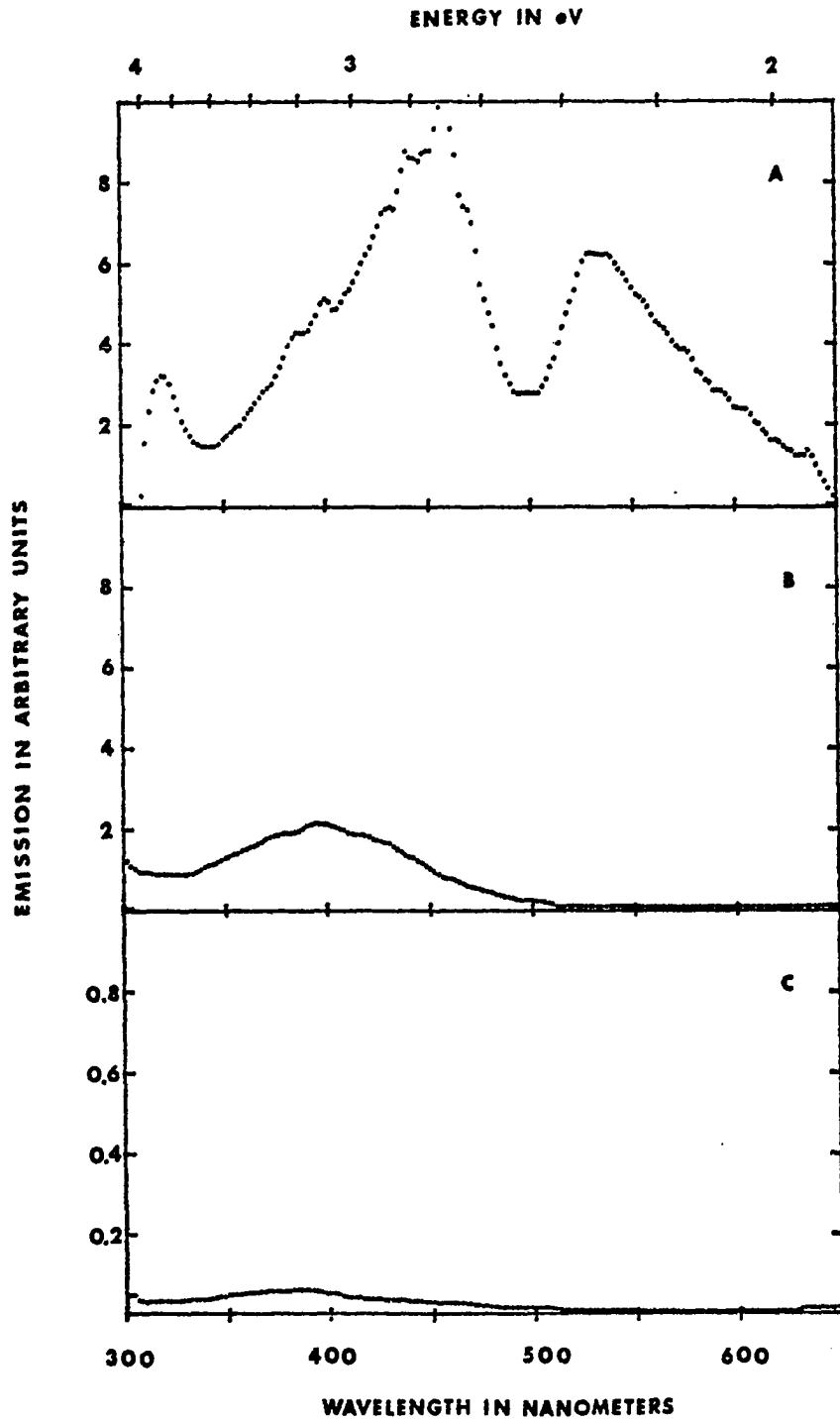


Figure 19. Exoelectrons detected with: (A) no magnetic field, (B) 5 gauss magnetic field, and (C) 8 gauss magnetic field.

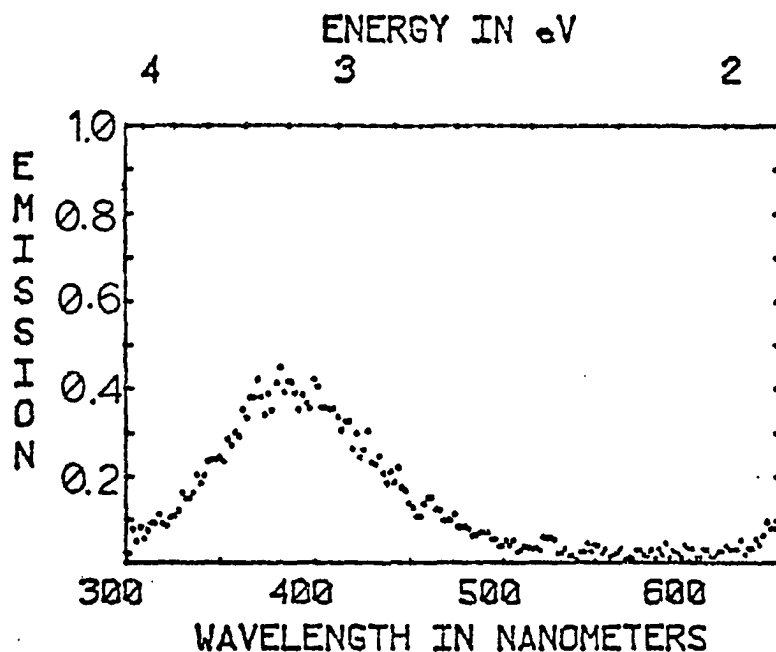


Figure 20. Exoemission spectrum for electron energies greater than about 0.5 eV. Energy discrimination by earth's magnetic field.

trum of a colored crystal changes the spectrum to some degree depending on the intensity of light and exposure time. To investigate this issue a KCl single crystal was irradiated with 3 keV at 10 μ a for 10 seconds twice in succession and its OSEE spectrum was run first from red to blue (Figure 21(B)) and then from blue to red (Figure 21(D)) using a monochromator slit width of 0.1 mm. Instrumental limitations prevented extending the spectrum far enough into the infrared to detect the R, M and N bands in KCl, however the effects of bleaching on the K, L₁ and 395 nm bands are clear.

Before each irradiation the crystal was bleached for 30 minutes with white light from the projector lamp. The bleached crystal spectra

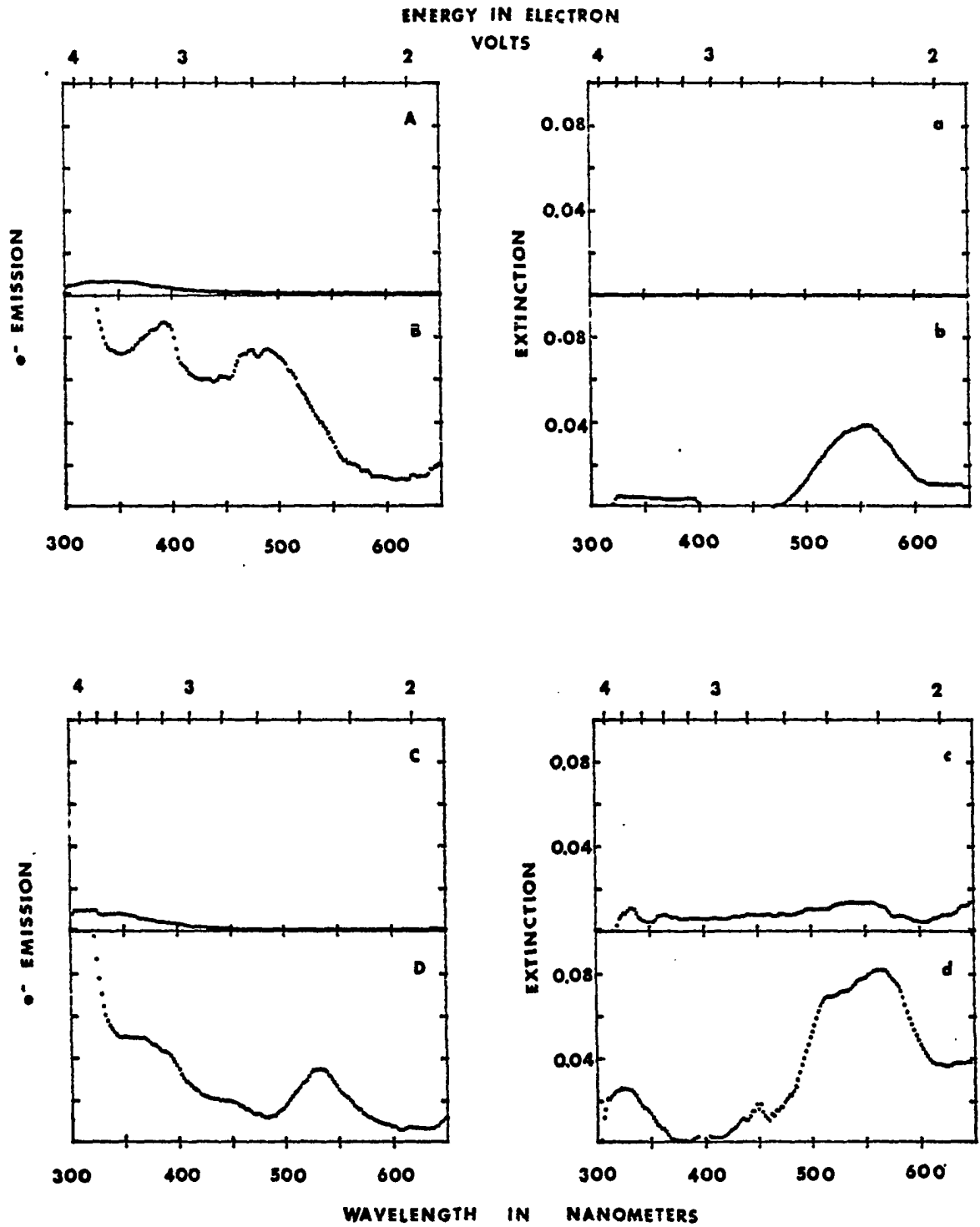


Figure 21. Exoemission (capital letters) and extinction (small letters) versus scan direction. (A) bleached crystal, red-to-blue; (B) irradiated crystal, red-to-blue; (C) bleached crystal, blue-to-red; (D) irradiated crystal, blue-to-red.

are shown in Figures 21(A) and 21(C). This was the same crystal as that shown in Figure 14 and therefore had been previously irradiated a sufficient number of times that the F-band emission was not detectable as a separate peak in the red-to-blue scan shown in Figure 21(B).

The blue-to-red scan of Figure 21(D) shows that exposure to short wavelength light has bleached the K emission band, and a distinct F-band has reappeared. If Figure 21(B) is superimposed upon Figure 21(D) the F-band in 21(D) will be seen to fit underneath the long wavelength tail of the K-band in 21(B). On the other hand the absorption spectra of Figures 21(b) and 21(d) behave in the opposite manner. The red-to-blue scan resulted in a normal F-band absorption, while the blue-to-red scan caused an increase in the K-band absorption and an apparent splitting of the F-band. This behavior is difficult to understand.

To investigate the rate of bleaching of the OSEE spectra a KCl crystal was irradiated with a 3 keV 100 μ a electron beam for 10 sec. This exposure was found to produce an exoemission spectrum which could be scanned several times in succession without bleaching completely away. This experiment was repeated twice on the same crystal by first irradiating and then scanning six spectra in succession all in the same direction. The results of the red-to-blue scans are shown in Figure 22, and the blue-to-red scans are in Figure 23. The areas under the emission peaks and under the optical extinction curves were calculated by summing the detected counts between 480 nm and 600 nm. The areas were then normalized to their respective values obtained on the first scan. These are listed in Table 1 and plotted in Figure 26. Circles represent the normalized area under the exoemission peaks while X's represent the area

under the K and F absorption bands. Error bars of $\pm 3\%$ reflect the random fluctuations in lamp intensity.

The freehand curves of Figure 25 show that in the case of the red-to-blue scans the OSEE and the optical extinction bleach at approximately the same rates while the blue-to-red scan causes the OSEE to disappear much more rapidly. In both cases the optical absorption peak is seen to increase after about 5 scans. This probably corresponds to a breaking up of F-aggregate centers. In all cases a simple exponential least squares fit is insufficient to reproduce the data. (See Figure 24.)

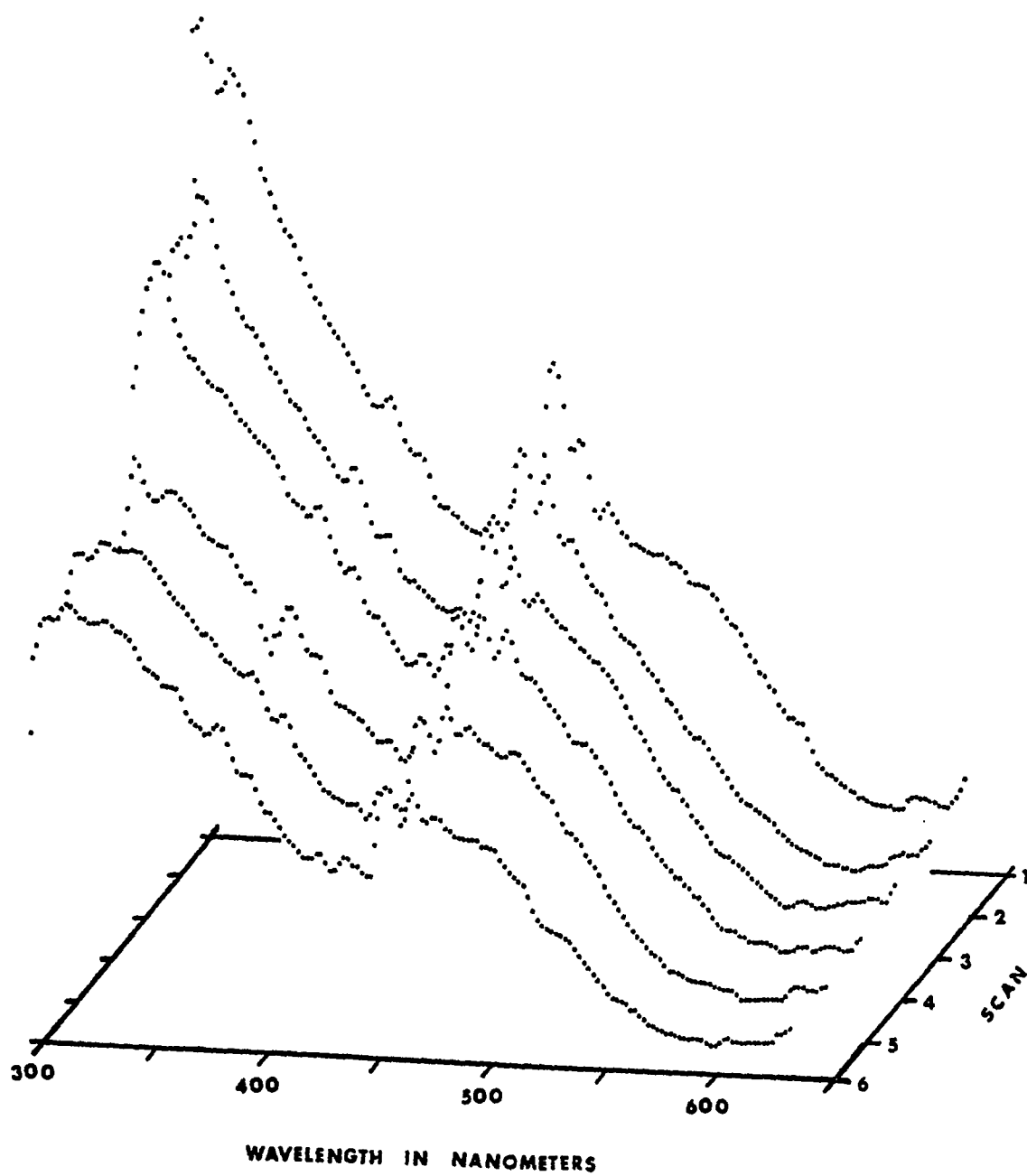


Figure 22. Exoemission spectrum versus scan number, red-to-blue.

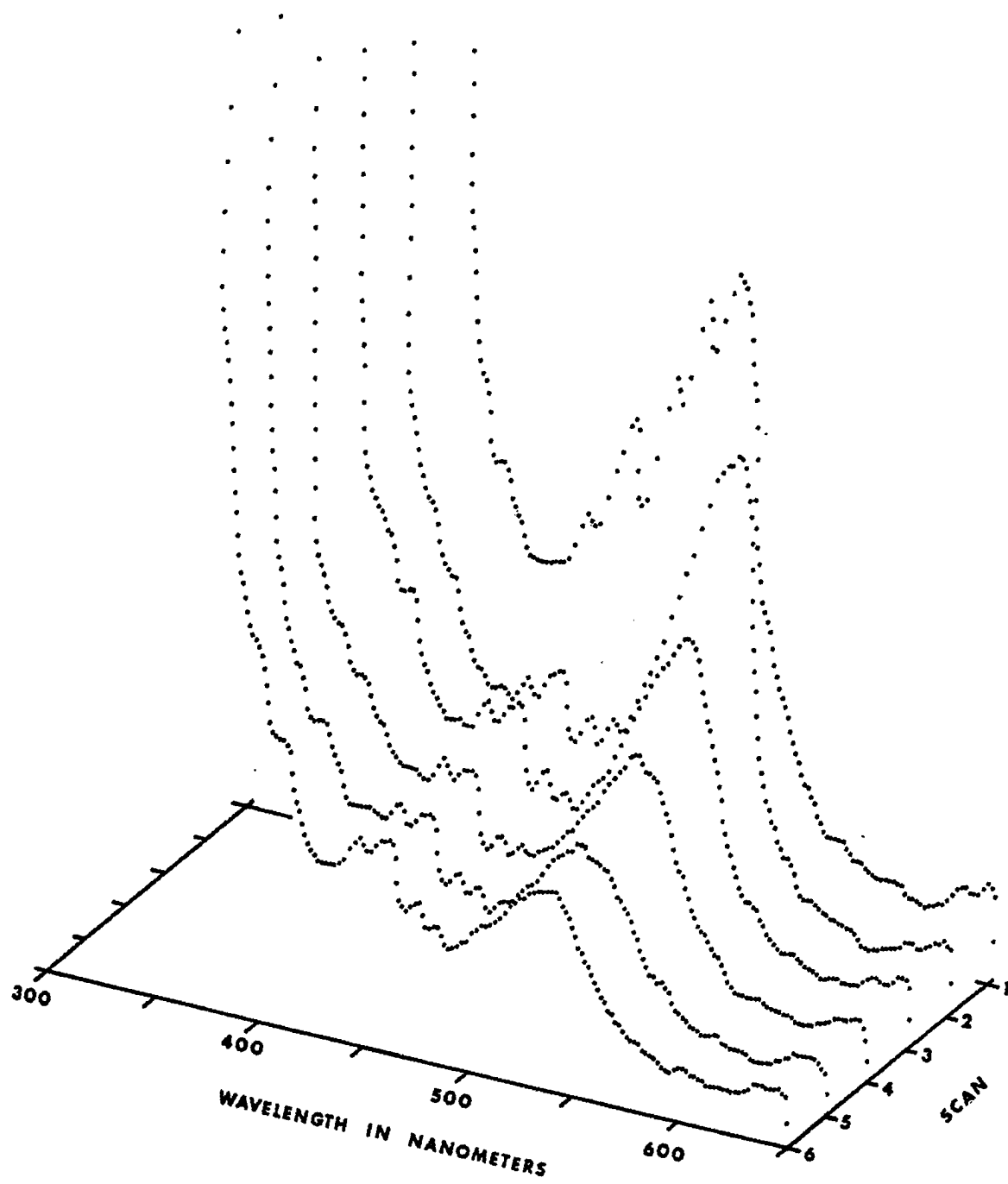


Figure 23. Exoemission spectrum versus scan number, blue-to-red.

TABLE 1

RED-TO-BLUE

Scan Number	Area Under OSEE Peak	Area Under Absorption Peak
1	100%	100%
2	85%	82%
3	84%	76%
4	79%	--
5	71%	57%
6	62%	62%

BLUE-TO-RED

1	100%	100%
2	60%	93%
3	39%	88%
4	32%	85%
5	26%	91%
6	25%	88%

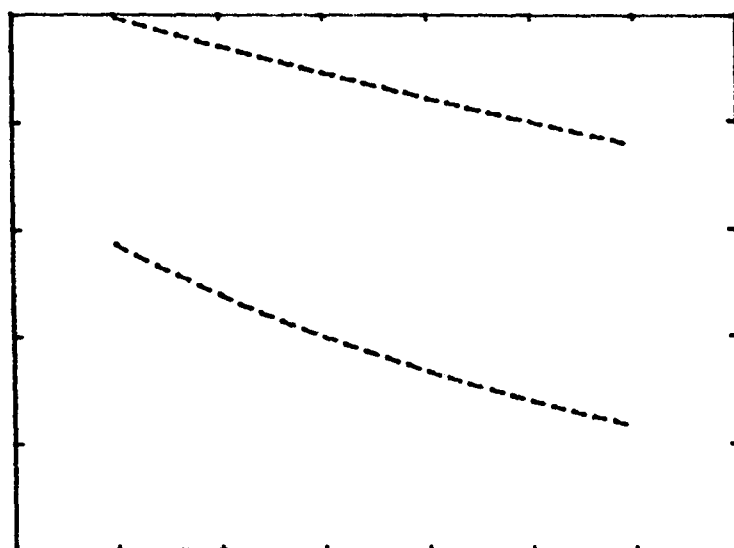
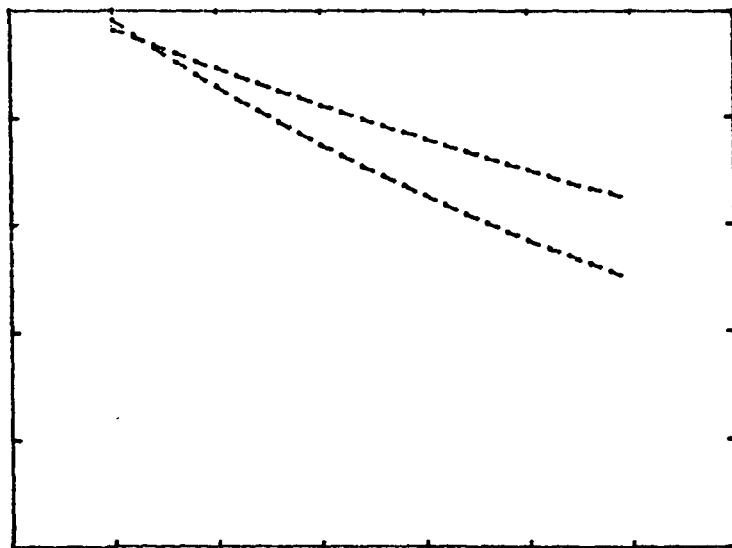


Figure 24. Exponential least squares fits to decay of absorption and emission peaks for (A) red-to-blue, and (B) blue-to-red scans.

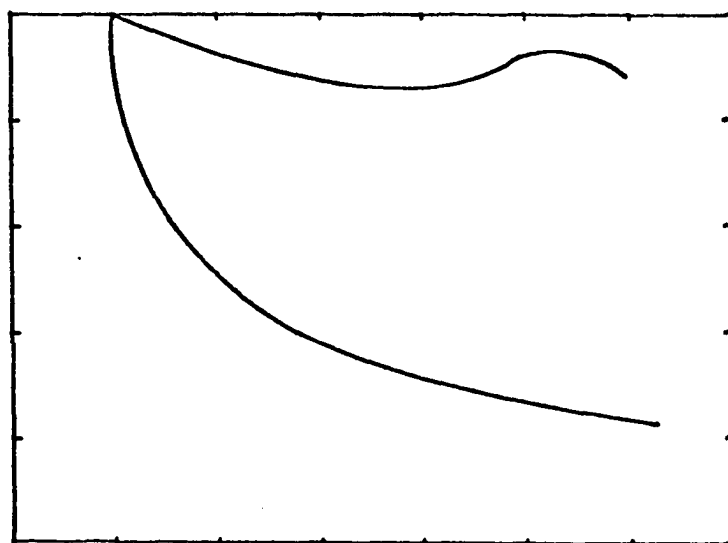
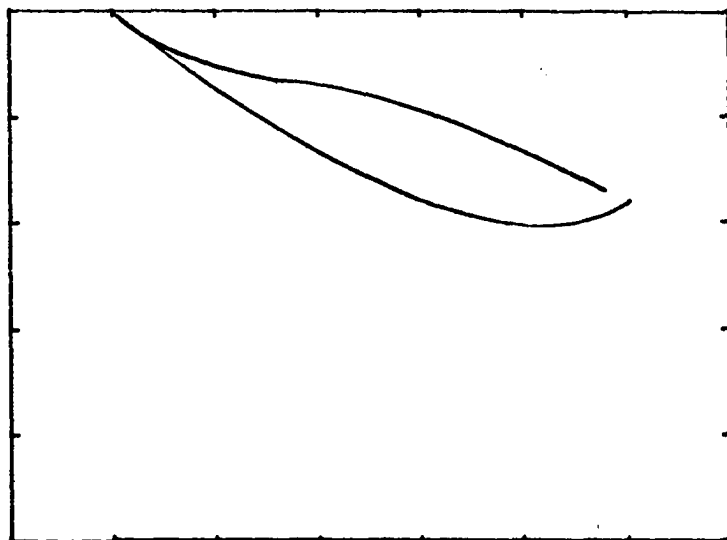


Figure 25. Freehand fits to decay of absorption and emission peaks for (A) red-to-blue, and (B) blue-to-red scans.

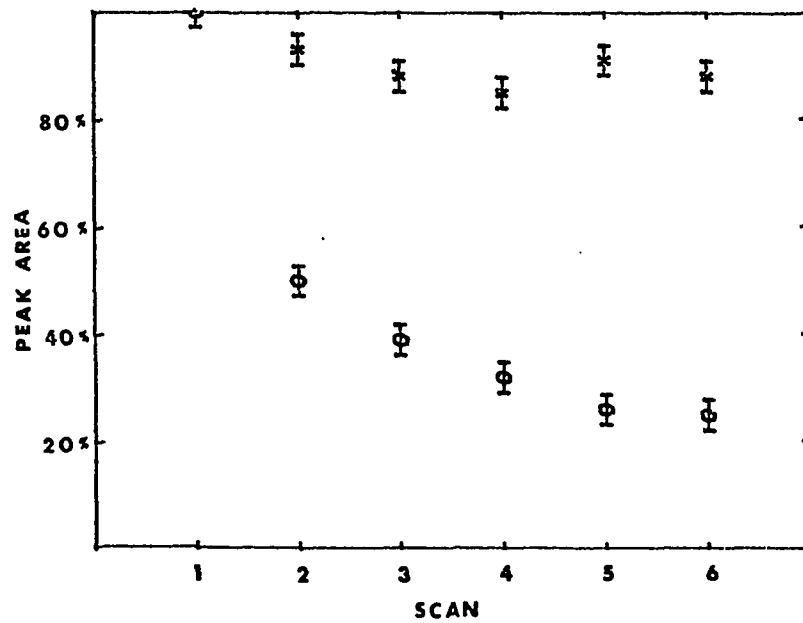
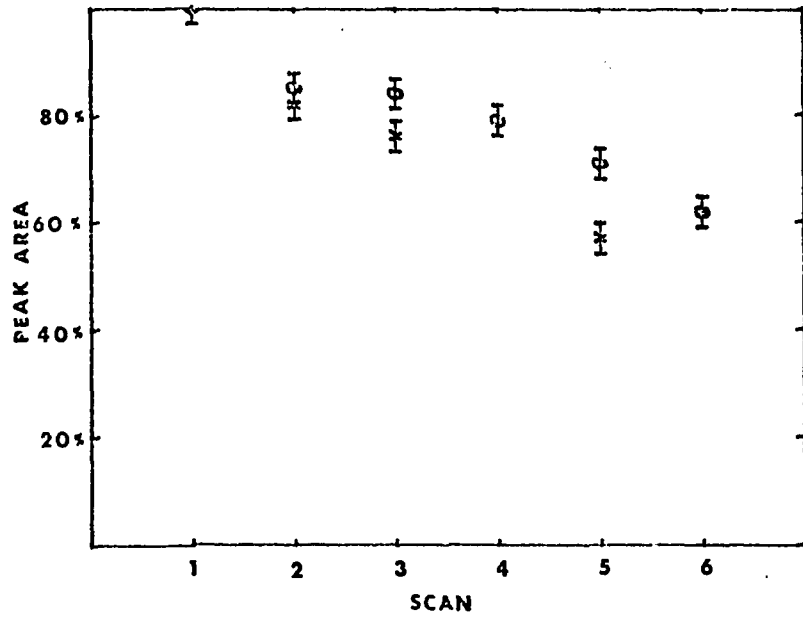


Figure 26. Decay data for absorption (x) and emission (o) peaks.

(A) red-to-blue, and (B) blue-to-red scans

CHAPTER V

DISCUSSION

It is clear from these results that optically stimulated exoelectron emission is indeed a very sensitive technique for studying color centers as was pointed out by Petrescu.¹⁴ To a first approximation it is true that the use of polycrystalline samples and gas flow techniques do not destroy the exoemission signal. However the present work demonstrates that both the magnitude and wavelength of the OSEE peaks are affected by the surface properties of the sample. Moreover, high vacuum and channel electron multiplier techniques greatly increase the sensitivity of this type of experiment.

Simultaneous measurement of optical absorption and OSEE is useful in identifying OSEE peaks and studying their behavior under various treatments. It is clear however that a double beam spectrophotometer would be preferable because of the weak colorations produced by low energy electron beams. The K and L absorption bands were essentially invisible in the absorption spectrum but they are easily detected by OSEE.

Many investigators now accept Petrescu's conclusion that the correspondence between exoemission peaks and optical absorption peaks indicates that the exoelectrons originate in the bulk defects of the crystal.³⁶ If this interpretation is correct then the present experiment

has established the presence of the K and L_1 exoemission bands in KCl as well as an emission band located at 395 nm. It has been demonstrated that electrons emitted directly from the F and K bands have kinetic energies less than about 0.5 eV while those emitted from the L_1 -band and the 395 nm band have energies between about 1.0 and 2.5 eV. This indicates that F and K band electrons are emitted from a lower lying (more tightly bound) energy state.

Based upon previous experiments which have been summarized by Fowler²¹ plus the information about the 395 nm band obtained from the present experiment, it is possible to propose an energy level diagram for the F-center in KCl. The proposed scheme is shown in Figure 27. Wild and Brown³⁴ have established the energy of the lowest band-to-band transitions, E_G^0 , at 8.5 eV corresponding to a step in the photoconductivity curve. This represents the minimum energy required to promote a valence electron to the bottom of the conduction band, and so establishes the band gap energy.

Photoelectron emission data of Taft and Philipp³⁷ show that 8.7 eV is required to remove a valence electron from the crystal. This places the vacuum level only 0.2 eV above the bottom of the conduction band. This fact is important for electron emission because it indicates that most electrons which are promoted into the conduction band will find themselves with enough energy to escape the crystal provided they are liberated near enough to the surface so that they do not undergo too many collisions before escaping. If the electrons in the conduction band obey Fermi-Dirac statistics then at room temperature approximately 0.06% will have thermal energies larger than 0.2 eV.

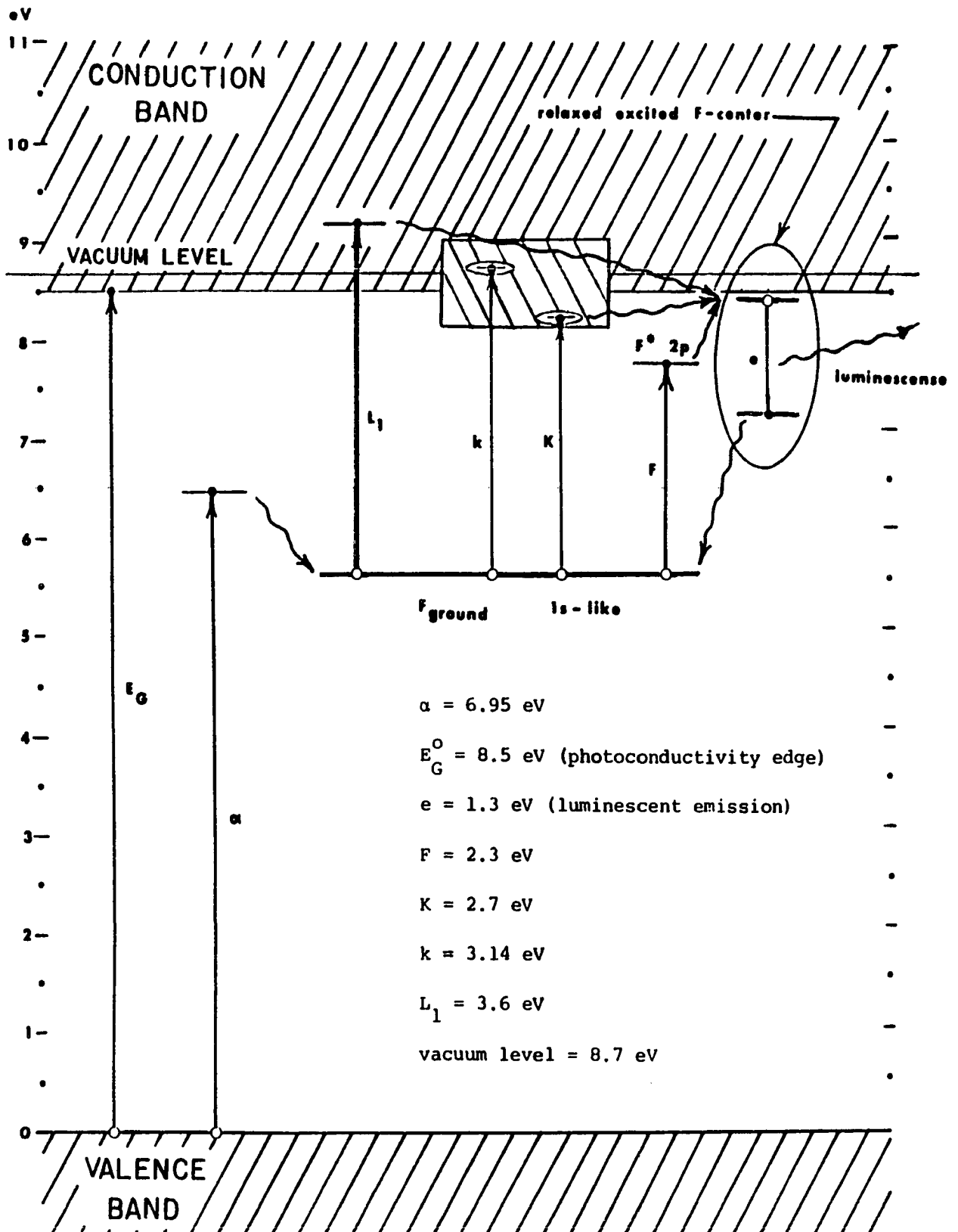


Figure 27. Proposed energy level scheme for F-center.

Since the F-center traps one electron, Mott and Gurney³⁰ have treated it theoretically as an analog to the hydrogen atom. They proposed that the F-absorption band arises from the $1s-2p$ transition of the trapped electron while the K-band arises from a superposition of $1s-np$, $n \geq 3$ transition. Smith and Spinolo³² have also pointed out the possibility that the K-band arises from more than one transition. This interpretation of the K-band is consistent with the appearance of the 395 nm OSEE emission band in the present experiment, and with the fact that in optical absorption spectra the K-band is found to have an extremely long high energy tail. Other calculations based upon refinements of the hydrogen atom model predict higher p-like states with energies in the range of the L-bands. (See Fowler.²¹)

If the F, K, k, and L_1 bands are all assumed to arise from transitions beginning from the same ground state, as this model suggests, then the question of the location of that ground state energy level with respect to the conduction band is important. This is not however an easy question to answer. One possibility might be to create ionized F-centers (halogen vacancies) and then measure the energy required to promote an electron from the valence band into the vacancy. This corresponds to a measurement of the α -absorption band, and is found to require 6.95 eV.²¹ It is clear however that this cannot be the location of the F-center ground state, since if it were, a subsequent stimulation of 2.3 eV in the F-band would raise the trapped electron to a total of 9.25 eV above the valence band. This would imply that electrons trapped at F-centers would all be liberated from the crystal when exposed to 540 nm (F-band) light--an event which does not occur. Therefore, while

the α -absorption at 6.95 eV does reflect the energy required to trap an electron at an F-center, it does not reflect the electron's energy once it has been trapped.

This can be understood in terms of the Stokes shift. The energy states of the halogen vacancy are determined solely by the charge distribution of the ions which surround the vacancy. Once an electron has been trapped at the vacancy, however, the charges surrounding the ions re-distribute to reflect the presence of an additional charge. Thus the lattice "relaxes" and the ground state energy level shifts by an undetermined amount.

Swank and Brown³⁸ measured the activation energy required to promote an electron from the excited state of the F-center into the conduction band. This measurement yielded a value of 0.14 eV, however excitation of the F-center electron must also result in a relaxation of the lattice and hence a Stokes shift. This 0.14 eV must represent the position of the first excited state after relaxation, and since it is not known how much energy is given up in the relaxation process, we still have not located the ground state level.

Wild and Brown³⁴ were the first to detect the 395 nm band which appeared in their photoconductivity data. Since this sudden rise in conductivity occurs in the high energy tail of the K-band where absorption is decreasing, its presence must indicate the opening of a new excitation channel with high transition probability. This led to the identification of the 395 nm band with the bottom of the conduction band and placed the F-center ground state at about 5.36 eV above the valence band. This interpretation is free of the relaxation problems of the previous

measurements because it represents a resonance in which the excited electron suddenly finds itself free from the effects of the F-center.

If this interpretation is correct, then the appearance of the 395 nm band in the OSEE spectrum is quite significant, since it seems to indicate that it is not the conduction band edge which should be identified with this transition, but rather the vacuum level. Electrons stimulated with 3.14 eV light not only find themselves free to leave the F-center, but also free to leave the crystal. Based upon this identification we place the F-center ground state at 4.45 eV above the valence band as shown in Figure 27.

If the level scheme of Figure 27 is correct then the mechanism by which exoelectrons are emitted from KCl is different for the F and K bands than for the k and L_1 bands. In the case of the F and K bands a two-step process is required to free the trapped electron. Optical stimulation at these wavelengths is sufficient to raise the electron to an excited state, but more energy is required to raise it to the vacuum level. In the case of the F-band the required additional energy would consist of the 0.14 eV activation energy which is necessary to promote the electron from the relaxed excited F-state into the conduction band plus an additional 0.2 eV needed to reach the vacuum level. So the total activation energy is 0.34 eV. At room temperature about $2 \times 10^{-4}\%$ of the excited electrons can acquire this additional energy by thermal stimulation. This is a small fraction, but according to Soul and Tubbs²⁶ we expect the irradiated sample to contain $\sim 10^{19}$ F-centers per cubic centimeter.

In order to find the thermal activation energy required to free

an electron in the K-band we must know where the relaxed excited K-state lies with respect to the conduction band. Fowler²¹ has pointed out the results of several experiments in which the F-center was stimulated with K-band light and the luminescence emitted from the crystal was the same as the normal F-band luminescence. Therefore the relaxed excited K-state seems to be identical to the relaxed excited F-state. This fact is noted in Figure 27. It is also found that the L-states relax to the same excited state. Therefore exoemission from the K-band should have the same temperature dependence as the F-band emission.

Exoemission from the k and L_1 bands should not require thermal activation according to this model. Stimulation with k or L_1 band light should raise the trapped electron to excited states which lie within the conduction band and which are isoenergetic with vacuum states. In this case we would expect an auto-ionization of the excited center before relaxation occurs. This would result in an Auger-like emission process similar to the model of Tolpygo et al.²⁴

If this model of the F-center is correct we can predict that as the colored KCl crystal is cooled below room temperature the exoemission from the F and K bands should disappear simultaneously at some temperature where the necessary thermal activation energy is no longer available. However, exoemission from the k and L_1 bands should not disappear with lower temperature since these states are essentially auto-ionizing. This kind of behavior was seen in the photoconductivity data of Wild and Brown. A similar investigation of the exoemission spectrum at low temperatures would definitively establish whether or not the k-band should be identified with the vacuum level, and it should certainly be

the next step in investigating this phenomenon.

An interesting feature of the F-band emission can be seen in Figures 15 through 18. It was previously noted that the F-band exoemission peak appears to shift to longer wavelengths as the temperature of the crystal is increased. It is not merely the peak of the F-band which shifts, but the minimum on the high energy side of the peak shifts as well. At 30°C in Figure 18 photons of 2.4 eV are seen to produce an emission intensity which is about 75% of the maximum F-band intensity. However at 75°C in Figure 15 photons of 2.4 eV produce almost no exoemission even though more thermal energy is now available to the crystal. This must reflect the fact that lattice vibrations increase with temperature, and so increased motion of the ions surrounding the F-center causes a decrease in the energy of the F-center ground state. The same behavior has been observed in the optical absorption spectra, but to a much less marked degree.¹⁷

It should be pointed out that it has been tacitly assumed by most exoemission investigators that the presence of OSEE peaks which correspond to optical absorption features is proof of the bulk nature of the OSEE process.³⁶ While the present experiment seems to confirm that assumption and expand upon it, the surface condition of the crystal cannot be ignored. It is still not possible at the present time to rule out surface states or adsorbed gasses as a source of some exoemission features. Three features of the data taken in the present experiment have not been explained by the F-center model of Figure 27, and any theory which purports to explain the exoemission phenomenon must account for these data.

It was noted in Figures 11(C) through 11(E) that after initial irradiation of the crystal, a second spectral scan revealed that most of the exoemission features had disappeared (Figure 11(D)), however after sitting overnight undisturbed in vacuum at room temperature with no external light source new exoemission peaks appeared (Figure 11(E)). The new exoemission spectrum displays peaks near the stimulation energies of the freshly irradiated crystal, but the relative intensities of each peak and the exact wavelength of the peaks have changed dramatically. No mechanism for these changes has been proposed by the model of Figure 27, and the changes are not yet understood.

The dependence of the exoemission spectrum upon the direction of the spectral scan, as shown by Figure 21, also remains unexplained. As previously stated one would expect to see this sort of behavior only if the lifetimes of the populated states were of the same order of magnitude as the period of the spectral scan--in this case about 10 minutes. If the excited states were assumed to be thermally populated, and the stimulation energy of the light beam served only to free the excited electrons then it might be expected that the first emission band to be stimulated would produce the highest emission intensity, while succeeding bands would appear depleted. This process would require thermal stimulations on the order of 2 to 3 eV which, at room temperature, will occur with a probability of less than 10^{-33} . Moreover from Figure 21 it can be seen that the first peak scanned is not enhanced, but rather it is depleted with respect to those peaks subsequently scanned. So thermal population of the excited levels cannot explain the data either.

In discussing the thermal dependence of the exoemission shown in Figures 15 through 18 we have limited our discussion to the F and K bands which display the behavior expected. However the growth of the k and L_1 bands with temperature presents another problem for the F-center model, because these states should be auto-ionizing and should not require additional thermal excitation. This difficulty can only be overcome if we assume that the thermal energy serves to increase the probability that the auto-ionized electron will be able to diffuse to the surface of the crystal without losing a significant portion of its energy to collisions. This explanation is a problem in itself since at higher temperatures collisions should become more probable.

Finally, if the F-center model of the exoemission process is to be accepted, it will be necessary to study the exoemission spectrum of the KCl crystal as impurity atoms are doped into the lattice. Such a study would allow one to discover whether the double peak appearance of the F-emission band is really the result of impurity ions such as Na^+ sitting next to the F-center, or whether a different explanation is required.

REFERENCES

1. McLennan, J. C. Physikalische Zeitschrift v. 49 (1901) p. 704
2. Apker, L. and Taft, E. Physical Review v. 79 no. 6 (1950) p. 964
3. Kramer, J. Zeitschrift für Physik v. 133 (1952) p. 629
4. Becker, K. Solid State Dosimetry (1973, CRC Press, Inc.) pp 334
5. Brunsmann, U. and Scharmann, A. Physica Status Solidi v. (a)26 (1974) p. K123
6. De Muer, D. and Maenhout-van der Vorst, W. Physica v. 49 (1970) p. 157
7. Gordan, P. and Scharmann, A. Zeitschrift für Physik v. 217 (1968) p. 309
8. Lukirsky, P., Gudris, N., and Kulikowa, L. Zeitschrift für Physik v. 37 (1926) p. 308
9. Fleischmann, R. Zeitschrift für Physik v. 84 (1933) p. 717
10. Bohun, A. Czechoslovak Journal of Physics v. 4 (1954) p. 139
11. Bohun, A. Czechoslovak Journal of Physics v. 5 (1955) p. 64
12. Sujak, B. Acta Physica Polonica v. 12 (1953) p. 241
13. Petrescu, P. Physica Status Solidi v. 3 (1963) p. 950
14. Petrescu, P. Physica Status Solidi v. 9 (1965) p. 539
15. Petrescu, P. Physica Status Solidi v. 29 (1968) p. 333
16. Petrescu, P. Physica Status Solidi v. 29 (1968) p. K1

17. Markham, J. "F-Centers in Alkalai Halides" Solid State Physics: Advances in Research and Applications Supplement 8 (1966, Academic Press, Inc.) pp 37-57
18. Townsend, P. and Kelly, J. Colour Centers and Imperfections in Insulators and Semiconductors (1963, Crane, Russak and Co.) pp 179-189
19. Pooley, D. Solid State Communications v. 3 (1965) p. 241
20. Hersh, H. Physical Review v. 148 (1966) p. 928
21. Fowler, W. Physics of Color Centers (1968, Academic Press) pp 87-93
22. Randall, J. and Wilkins, M. Proceedings of the Royal Society of London serial A v. 184 (1945) p. 366
23. Bohun, A. PTB-Mitteilungen v. 5 (1970) p. 320
24. Tolpygo, E., Tolpygo, K., and Sheinkman, M. Izvestiya Akademii Nauk SSSR, Seriya Fizika v. 30 (1966) p. 1980
25. Sujak, B. Acta Physica Austriaca v. 10 (1957) p. 460
26. Soul, P. and Tubbs, M. Solid State Communications v. 7 (1969) p. 397
27. Spangenberg, K. Vacuum Tubes (1948, McGraw-Hill, Inc.) p. 171
28. Townsend, P. and Kelly, J. Physics Letters v. 26A no. 4 (1968) p. 138
29. Palmberg, P. and Rhodin, T. Journal of Physics and Chemistry of Solids v. 29 (1968) p. 1917
30. Mott, N. and Gurney, R. Electronic Processes in Ionic Crystals (1940, Oxford University Press) p. 114
31. Konitzer, J. and Markham, J. Physical Review v. 107 no. 3 (1957)

p. 685

32. Smith, D. and Spinolo, G. Physical Review v. 140 no. 6A (1965)
p. A2121
33. Nakazawa, F. and Kanzaki, H. Journal of the Physical Society of Japan v. 20 (1965) p. 468
34. Wild, R. and Brown, F. Physical Review v. 121 (1961) p. 1296
35. Malmstadt, H. and Enke, C. Digital Electronics for Scientists
(1969), W. A. Benjamin, Inc.) p. 226
36. Brunsmann, U. and Scharmann, A. Physica Status Solidi v. (a)43
(1977) p. 519
37. Taft, E. and Philipp, M. Physics and Chemistry of Solids v. 3
(1957) p. 1
38. Swank, R. and Brown, F. Physical Review Letters v. 8 (1962) p. 10

APPENDIX 1

PRESETABLE UP/DOWN COUNTER

The presetable up/down counter is constructed using Signetics N74192 binary coded decimal (BCD) synchronous counter chips. Six of these chips are cascaded together as shown in Figure 27 to form a six digit decimal counter. Cascading is obtained by connecting the borrow output (pin 13) to the count down input (pin 4) and the carry output (pin 12) to the count up input (pin 5) of each successive counter. The clear inputs (pin 14) are connected together and held at ground by a resistor.

Pushbutton S_1 will momentarily apply +5 VDC to the clear line and preset all of the counters to zero. To preset the scalar to some number other than zero the data input lines (pins 1, 9, 10, 15) of each 74192 are connected to BCD thumbwheel switches S_3 through S_8 . The counters will be preset to the six digit number appearing on the thumbwheel switches whenever the load lines (pins 11) are brought to ground by S_2 .

The content of each counter is displayed on a MAN7 seven segment LED display. Each MAN7 display is driven by its own 7447 decoder/driver, so each decimal digit is displayed separately from every other digit, i.e. the displays are not multiplexed. Each 7447 provides a ripple blanking output signal at pin 4 to the ripple blanking input (pin 5) of the next lower digit. This feature provides for the suppression of lead-

ing zeros. Moreover, the ripple blanking output of the least significant digit provides a $\overline{\text{ZERO}}$ signal to the control logic which stops the counter when all digits are zero.

The input signal is inverted and gated by NAND gate number 1 in Figure 28. As long as the counter is in the counting mode (i.e., COUNT = logical 1) the input pulses will pass through gate 1 and be routed by S_9 to either the COUNT UP or COUNT DOWN inputs of the 74192 chips. When the counter is in the stop mode (COUNT = 0) gate 1 is disabled and no more input pulses can reach the counters.

Whether the counter is in its counting mode or its stop mode is determined by the state of the D-type flip-flop in Figure 28. If $Q=1$ the device is counting; if $Q=0$ it is stopped. The counting mode is begun by pressing S_{11} to preset the flip-flop to $Q=1$. Counting can be stopped in three ways. If S_{10} is closed the flip-flop will clear and counting stops. Likewise an external signal can be applied to the STOP INPUT to clear the flip-flop. Counting will cease automatically when all counters reach zero because the $\overline{\text{ZERO}}$ signal from the ripple blanking output will cause NAND gate 2 to go high and provide a clock pulse to the flip-flop, changing its state to $Q=0$.

The Q and \bar{Q} signals from the flip-flop are output from the counter to provide gate levels for controlling external equipment. Moreover Q and \bar{Q} also trigger two 74121 multivibrators (not shown) to provide start and stop output pulses from the counter.

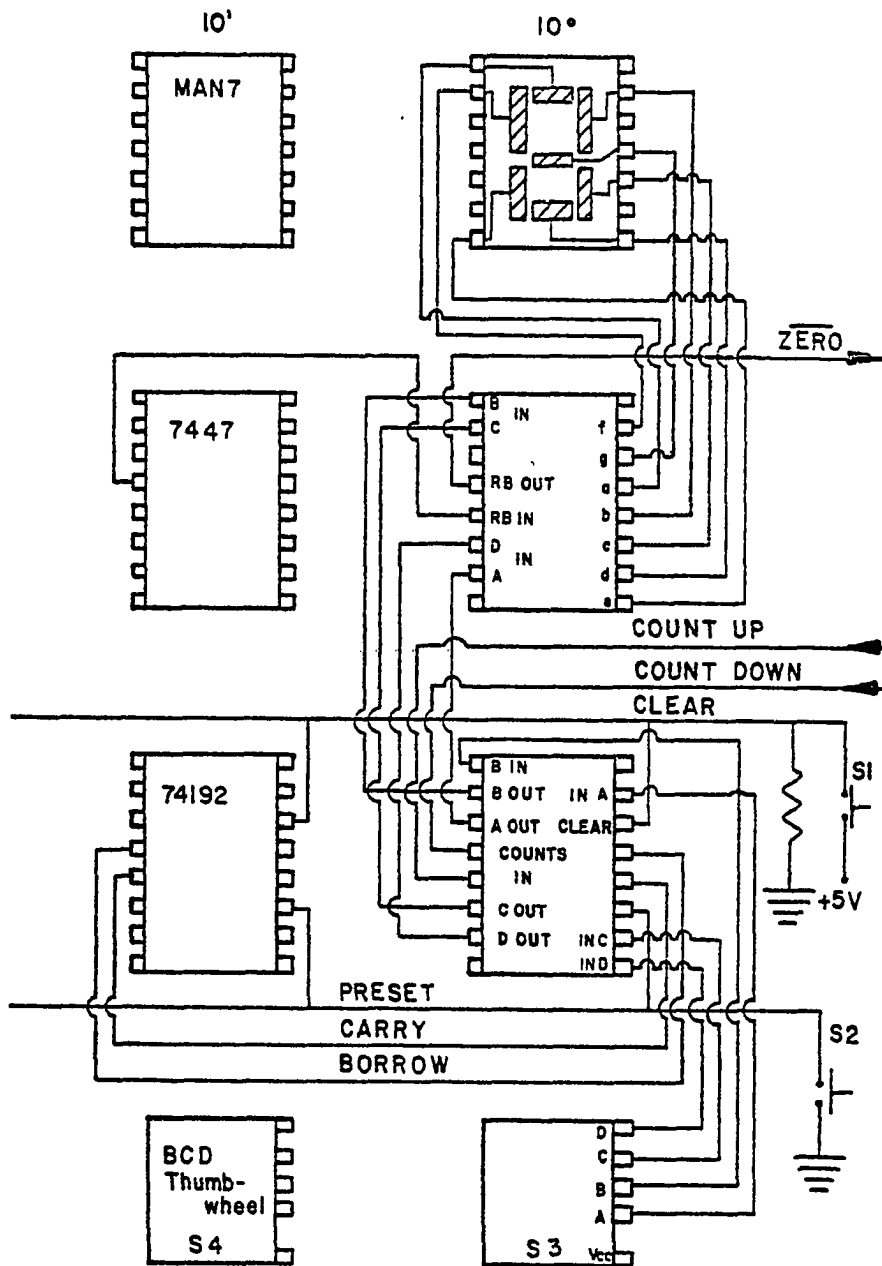


Figure 28. Presetable up/down counter.

APPENDIX 2

VOLTAGE CONTROLLED OSCILLATOR

The voltage controlled oscillator (VCO) circuit is used to interface the Kiethley model 610C multimeter with the multichannel analyzer when measuring optical absorption spectra or with the presetable up/down counter when measuring irradiation doseage. This VCO is constructed around a Raytheon RM4151 voltage-to-frequency integrated circuit chip. The particular circuit shown in Figure 29 provides the features of: (1) differential input, (2) input voltage range adjustable from 0-1 VDC to 0-10 VDC, (3) output frequency range 0-10 kHz, (4) frequency linearity of 0.05%.

The input stage of the VCO is a standard differential amplifier built around IC1, an LM308 operational amplifier. This amplifier provides a negative output voltage proportional to the difference between its input voltages. The inputs are protected against reversed polarity by diodes D_1 and D_2 . Resistors R_6 and R_8 form a double potentiometer which adjust the amplifier gain from 1 to 10.

The RM4151 voltage-to-frequency chip consists of three sections as shown in Figure 30. In normal operation the input voltage at pin 7 is compared to a reference voltage at pin 6 (established by R_{16} and R_{17}). If the input voltage is larger than that of pin 6 then the voltage

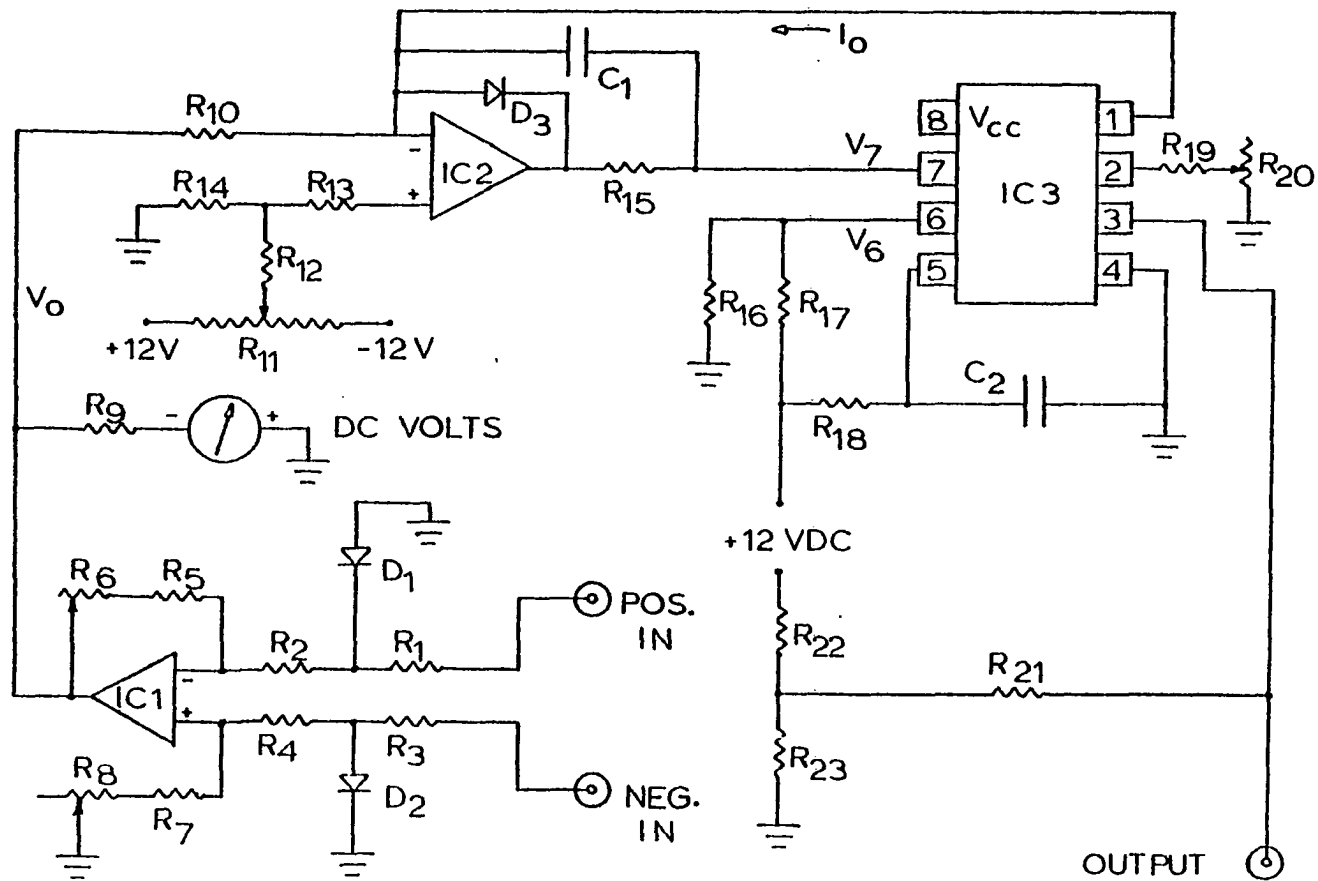


Figure 30. Voltage Controlled Oscillator Circuit.

TABLE 2
VOLTAGE-TO-FREQUENCY CONVERTER

$C_1 - 0.005 \mu f$	$R_{10} - 100 \text{ k}\Omega$
$C_2 - 0.01 \mu f$	$R_{11} - 10 \text{ k}\Omega$
$D_1, D_2, D_3 - 1N914$	$R_{12} - 100 \text{ k}\Omega$
	$R_{13} - 100 \text{ k}\Omega$
$R_1 - 100 \Omega$	$R_{14} - 500 \Omega$
$R_2 - 8.2 \text{ k}\Omega$	$R_{15} - 100 \Omega$
$R_3 - 100 \Omega$	$R_{16} - 10 \text{ k}\Omega$
$R_4 - 8.2 \text{ k}\Omega$	$R_{17} - 5.6 \text{ k}\Omega$
$R_5 - 8.2 \text{ k}\Omega$	$R_{18} - 6.8 \text{ k}\Omega$
$R_7 - 82 \text{ k}\Omega$	$R_{19} - 12.1 \text{ k}\Omega$
$R_8 - 8.2 \text{ k}\Omega$	$R_{20} - 10 \text{ k}\Omega$
$R_9 - 82 \text{ k}\Omega$	$R_{21} - 5.6 \text{ k}\Omega$
$R - 150 \text{ k}\Omega$	$R_{22} - 1.2 \text{ k}\Omega$
	$R_{23} - 1 \text{ k}\Omega$

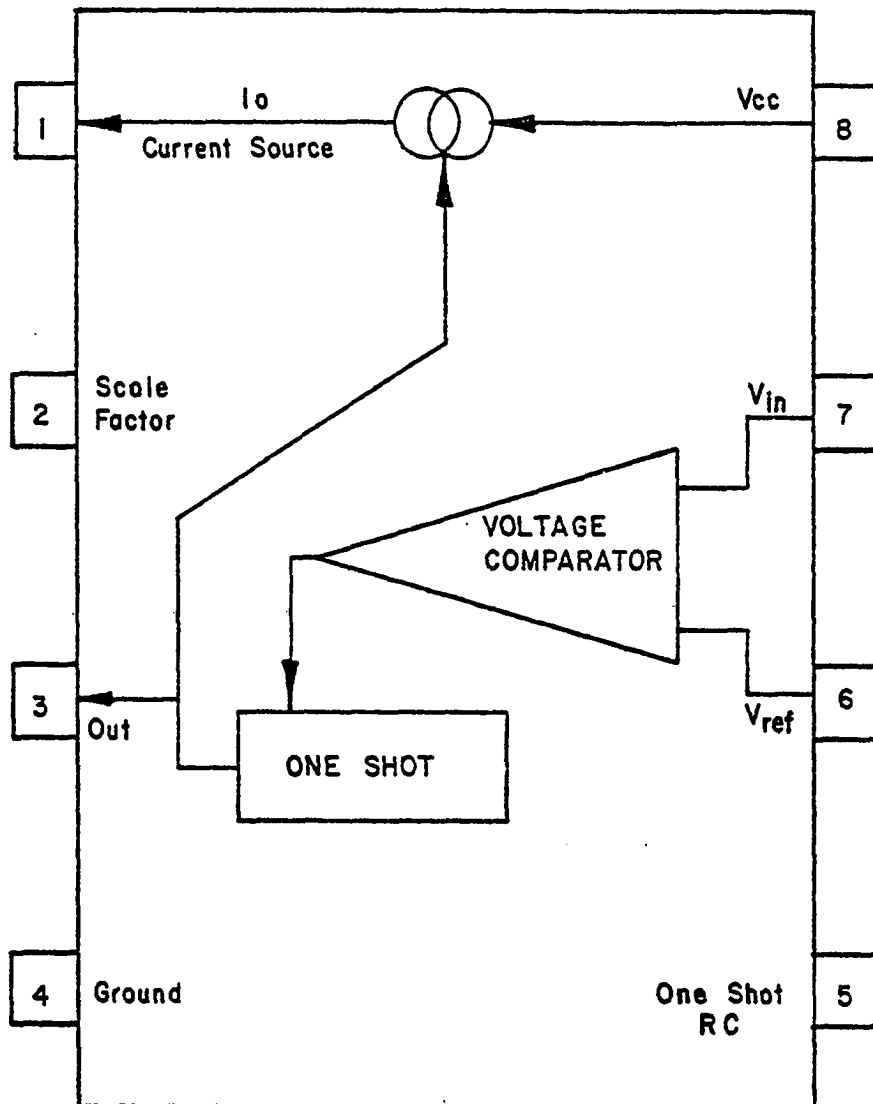


Figure 31. Raytheon RM 4151 Voltage to Frequency Chip.

comparator triggers the one-shot which provides an output pulse to pin 3. This pulse also triggers a current source within the chip which supplies an amount of charge $Q = I_0 T$ (where T is the period of the one-shot) to pin 1. This charge is used in the external circuitry to reduce the input voltage at pin 7 and thus disable the one-shot.

This voltage-to-frequency chip is interfaced to the input differential amplifier by a voltage integrator composed of IC2 and associated components. The negative voltage from IC1 (V_0) charges capacitor C_1 and provides a positive voltage at pin 7 of IC3 (V_7). As long as $I_0 \neq 0$ we can write:

$$V_7 = - \frac{1}{R_{10} C_1} \int V_0 dt$$

As stated earlier, when $V_7 > V_6$ current begins to flow from pin 1 onto capacitor C_1 which reduces V_1 below V_0 . This causes V_7 to fall below V_6 and turns off I_0 . With I_0 off the voltage at pin 7 will begin to rise once again according to the equation above until V_7 is again larger than V_6 , and the process repeats. From the equation it is clear that V_7 will increase more rapidly in time as V_0 increases and so the rate of firing of the one-shot will depend upon V_0 .

Diode D_3 insures that V_7 never becomes negative. Resistors R_{21} , R_{22} , R_{23} establish the output logic pulse level at +5 VDC. Resistor R_{18} and capacitor C_2 establish the period of the one-shot at about 14 kHz. Resistors R_{11} through R_{14} establish the zero voltage for the integrator circuit, and R_{19} , R_{20} determine the magnitude of current I_0 .

APPENDIX 3

MONOSTABLE DATA GATE

The monostable gate circuit provides a means for eliminating the problems which arise because the channel advance pulses from the monochromator are not equally spaced in time. This circuit consists of a 74121 monostable multivibrator which when triggered by the channel advance pulse from the monochromator provides a gateing signal whose duration in time depends only upon the RC time constant established by resistor R_1 (20 k Ω) and capacitor C_1 (22 μ f) or C_2 (82 μ f).

The channel advance pulse from the phototransistor mounted in the monochromator is inverted and amplified by a 741 operational amplifier. This amplifier is biased by means of resistors R_4 and R_5 to have a quiescent output voltage of +5 VDC. Each channel advance pulse from the monochromator then causes the output level of the operational amplifier to drop to zero volts. This triggering level is TTL compatible. It is re-inverted by means of NAND gate number 1 and output to be used as the channel advance command signal for the multichannel analyzers.

The inverted trigger signal is also fed to the Schmidt trigger input of the 74121 monostable multivibrator. When the trigger command occurs the monostable output, O, goes to logic level 1 and remains at this level for a time determined by the RC constant of the circuit. This time constant must be re-adjusted each time the scan speed of the mono-

chromator is changed.

The Q output of the 74121 provides a gate signal to a pair of data gate circuits similar to that described by Malmstadt and Enke.³⁵ These data gates have the property that a data pulse received simultaneously with the rising edge of the gate signal will be ignored by the circuit, while a data pulse which has already begun when the falling edge of the gate signal occurs, will pass undisturbed.

In this way the OSEE signal from the channeltron and the light intensity signal from the photomultiplier can be gated on and off simultaneously and will be passed to the multichannel analyzers for the same length of time between each channel advance pulse supplied by the monochromator. Moreover, data pulses which occur at the beginning or at the end of the channel advance pulse will not be distorted by the gate.

This circuit was mounted in a standard NIM bin module and the +5 VDC necessary to operate the logic gates of this circuit was developed from the +12 VDC supply of the NIM bin by means of an LM309 solid state voltage regulator.

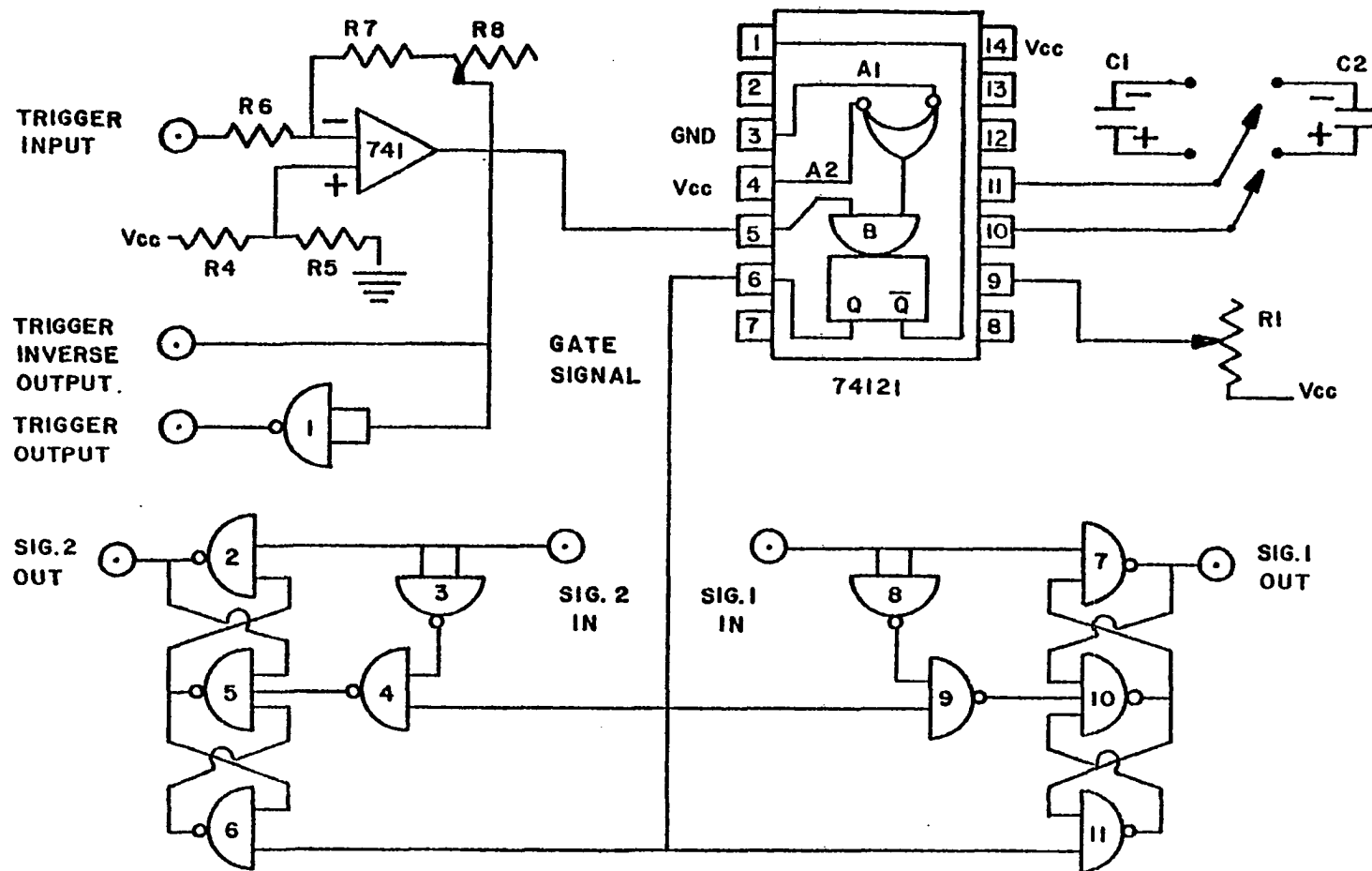


Figure 32. Monostable Data Gate.

TABLE 3
MONOSTABLE GATE

$C_1 - 22 \mu f$

$C_2 - 82 \mu f$

$R_1 - 20 k\Omega$ 10 turn

$R_4 - 8.2 k\Omega$

$R_5 - 1 k\Omega$

$R_6 - 8.2 k\Omega$

$R_7 - 8.2 k\Omega$

$R_8 - 82 k\Omega$

APPENDIX 4

TTL RELAY

In order to allow the presetable up/down counter to control the monochromator scan motor the TTL relay circuit in Figure 32 was constructed. When the counter enters its counting mode the gate output signal goes from zero to +5 VDC. When this voltage is applied to resistor R_1 it conducts about 25 ma of current through the gate of triac T_1 which causes T_1 to turn on.

Resistor R_2 establishes a 35 volt potential across trigger diode D_1 as soon as T_1 starts conducting. This 35 volts is sufficient to make D_1 conduct and fire triac T_2 . Thus the relay is energized and supplies power to the monochromator. Capacitor C_1 is used to shift the phase of the a-c line voltage at D_1 . This phase shift insures that T_2 will continue to conduct while the line voltage passes through zero and thus prevents the relay from chattering. A neon lamp indicates when the relay is energized, and the logic circuitry may be bypassed by the manual on/off switch.

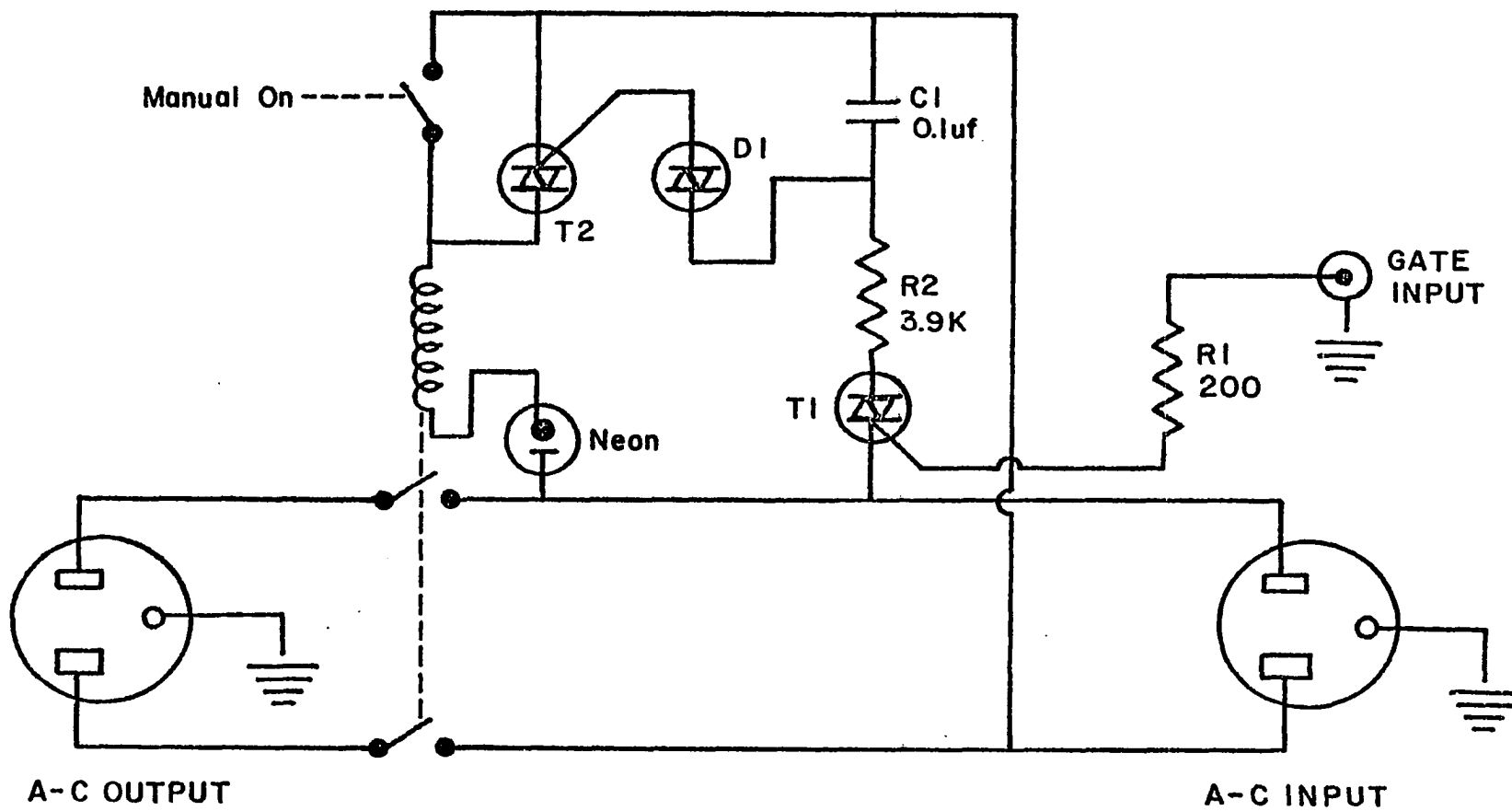


Figure 33. TTL Relay Circuit.

APPENDIX 5

DATA ANALYSIS PROGRAMS

Data analysis was performed on the Tektronix 4051 minicomputer. The two programs listed in Tables 4 and 5 were used to transfer data sets from the MCA's into the minicomputer and to normalize the data. These programs are written in the 4051 version of the BASIC programming language, and several of the commands used are machine dependent. Both programs utilize the user definable keys (UDK) of the Tektronix computer.

The data transfer program of Table 4 allows three data sets to be transferred into random access memory (RAM) and then be stored on magnetic tape. The format used for creating a data file on tape consists of a character variable containing the name of the data set, three integer variables specifying the number of points in the data set, the wavelength of the first point, and the distance between successive points on the wavelength scale, and an array, usually of length 177, containing the data. The array is assumed to be arranged in order of increasing wavelength with the first entry corresponding to the shortest wavelength.

Statement numbers 4, 12, 16, 20, 24, 32, 36, and 40 are program entry points addressed by the UDK's numbered 1, 3, 4, 5, 6, 8, 9, and 10 respectively. Key number 1 initializes the program for transfer of

data from the MCA. The data set transferred will be labelled in RAM as array X, Y, or Z depending upon whether UDK number 3, 4, or 5 is pushed. Data stored in array X is taken in the order it is presented by the MCA, while data sotred in arrays Y and Z have their order reversed--corresponding to a spectrum scanned from red to blue--before storage. UDK number 6 prepares the computer to store the data sets onto tape, and either array X, Y, or Z will be stored depending upon whether UDK number 8, 9, or 10 is pushed.

Statement number 180 sets the data communication rate between the MCA and the computer to 2400 bits per second. Statement 190 sets the minicomputer's processor status word to recognize a space as a record separator, and the control L symbol as an end of file mark, and to delete no characters from the incoming data stream. Statement 200 commands the computer to perform an automatic erase screen action whenever a page full condition occurs. Statements 220 through 550 perform the data transfer task, and statements 560 through 870 store the data set onto magnetic tape.

The normalization program listed in Table 5 is used to correct the OSEE data to account for the incident light intensity, and to calculate the extinction coefficient from the transmitted light data. UDK number 1 initializes the program for extinction coefficient calculations and starts execution at statement 100. The incident light spectrum is retrieved from tape in steps 110 through 170 and the transmitted light spectrum is retrieved in steps 290 through 350. The extinction spectrum is then calculated by statements 450 through 510 and this new data set is stored on tape. Other operations allow individual data sets to be

scaled by a constant factor and shifted a few channels toward longer wavelengths in case synchronization should be lost.

UDK number 6 initializes the program for correction of OSEE data. The phototube response curve is retrieved from the first file of the data tape in steps 670 through 760, and the measured light intensity curve is read from tape by statements 779 through 870. Finally the raw OSEE data are input in steps 880 through 960, and the correction formula is applied in the loop 970 through 1030. Then the corrected data set is stored on tape.

PLEASE NOTE:

In all cases this material has been filmed in the best possible way from the available copy. Problems encountered with this document have been identified here with a check mark ✓.

1. Glossy photographs _____
2. Colored illustrations _____
3. Photographs with dark background _____
4. Illustrations are poor copy _____
5. Print shows through as there is text on both sides of page _____
6. Indistinct, broken or small print on several pages _____ throughout

7. Tightly bound copy with print lost in spine _____
8. Computer printout pages with indistinct print ✓ _____
9. Page(s) _____ lacking when material received, and not available
from school or author _____
10. Page(s) _____ seem to be missing in numbering only as text
follows _____
11. Poor carbon copy _____
12. Not original copy, several pages with blurred type _____
13. Appendix pages are poor copy _____
14. Original copy with light type _____
15. Curling and wrinkled pages _____
16. Other _____

University
Microfilms
International

300 N. ZEEB RD., ANN ARBOR, MI 48106 (313) 761-4700

TABLE 4

DATA TRANSFER PROGRAM

```

4 GO TO 100
12 J=1
13 GO TO 220
16 J=2
17 GO TO 220
20 J=3
21 GO TO 220
24 GO TO 560
32 J=1
33 GO TO 600
36 J=2
37 GO TO 600
40 J=3
41 GO TO 600
100 PAGE
110 K$="INVERTING MATRIX."
120 A$="PUSH #3 FOR FORWARD, #4 FOR REVERSE (Y), #5 FOR REVERSE (Z)"
130 PRINT A$
140 S=177
150 A1=3000
160 A2=20
170 DIM X(S),Y(S),Z(S),W(S)
180 CALL "RATE",2400,0,2
190 PRINT @37,0:32,12,130
200 PRINT @32,26:2
210 RETURN
220 GO TO J OF 230,300,430
230 INPUT %40:Q
240 INPUT %40:X
250 PRINT X
260 IF Q>0 THEN 880
270 PRINT "WHAT IS DATA SET NAME?"
280 INPUT M$
290 RETURN
300 INPUT %40:Q
310 INPUT %40:W
320 PRINT K$
330 Y(1)=W(1)
340 FOR K=2 TO S
350 Y(S+2-K)=W(K)
360 NEXT K
370 W=0
380 PRINT Y

```

```

390 IF Q=0 THEN 330
400 PRINT "WHAT IS DATA SET NAME?"
410 INPUT B$
420 RETURN
430 INPUT X40:G
440 INPUT X40:W
450 PRINT N$
460 Z(1)=W(1)
470 FOR K=2 TO 5
480 Z(S+2-K)=W(K)
490 NEXT K
500 W=0
510 PRINT Z
520 IF Q>0 THEN 630
530 PRINT "WHAT IS DATA SET NAME?"
540 INPUT C$
550 RETURN
560 D$="FLSH #8 TO STORE (X), #7 TO STORE (Y), #10 TO STORE (Z)"
570 PRINT D$
580 CALL "RATE",300,0,2
590 RETURN
600 GO TO J OF 610,650,690
610 N$=M$
620 W=X
630 GOSUB 730
640 RETURN
650 N$=B$
660 W=Y
670 GOSUB 730
680 RETURN
690 N$=C$
700 W=Z
710 GOSUB 730
720 RETURN
730 PRINT "WHICH FILE?"
740 INPUT F
750 FIND F
760 IF TYP(0)=0 THEN 790
770 PRINT "FILE ",F," IS NOT NEW!"
780 STOP
790 FIND F
800 MARK 1,LEN(N$)+16*(S+3)
810 FIND F
820 PRINT 833:N$
830 PRINT 833:S
840 PRINT 833:A1,A2

```

```
550 PRINT Q304A
560 RETURN
570 END
580 PRINT "Q="1Q
590 STOP
```

TABLE 5

DATA NORMALIZATION PROGRAM

```

4 GO TO 100
8 GO TO 110
16 GO TO 110
20 GO TO 290
24 GO TO 370
28 GO TO 770
40 GO TO 350
100 DIM X(177),Y(177),Z(177),W(177)
110 PRINT "REFERENCE LAMP FILE?"
120 INPUT F
130 FIND F
140 INPUT @33:N$
150 INPUT @33:B
160 INPUT @33:A1,A2
170 INPUT @33:X
180 M1=0
190 FOR I=1 TO S
200 IF M1=>X(I) THEN 230
210 M1=X(I)
220 J=I
230 NEXT I
240 PRINT M1,J
250 PRINT N$
260 PRINT "DIVIDE BY?"
270 INPUT D
280 X=X/D
290 PRINT "DENOMINATOR FILE?"
300 INPUT F
310 FIND F
320 INPUT @33:N$
330 INPUT @33:B
340 INPUT @33:A1,A2
350 INPUT @33:Y
360 M2=0
370 FOR I=1 TO S
380 IF M2=>Y(I) THEN 410
390 M2=Y(I)
400 K=I
410 NEXT I
420 PRINT M2,K
430 PRINT "SHIFT HOW MANY?"
440 INPUT P
450 FOR I=1 TO S

```

```

460 IF I=P<> THEN 470
470 Z(I)=LET(X(I),Y I)
480 GOTO 510
490 IF I=PI THEN 470
500 Z(I)=LET(X(I),Y(I,P))
510 NEXT I
520 PRINT "FILE?"
530 INPUT G
540 PRINT "DATA SET NAME?"
550 INPUT Z$
560 FIND G
570 IF TYP(0)<>0 THEN 1190
580 FIND G
590 MARK 1-80+179*16
600 FIND G
610 PRINT @33:Z$
620 PRINT @33:G
630 PRINT @33:A1,A2
640 PRINT @33:Z
650 CLOSE
660 RETURN
670 INIT
680 DIM X(177),Y(177),Z(177),W(177),V(256)
690 FIND 1
700 INPUT @33:N$
710 INPUT @33:G
720 INPUT @33:A1,A2
730 INPUT @33:V
740 FOR I=1 TO 177
750 X(I)=V(I+24)
760 NEXT I
770 PRINT "LAMP REFERENCE?"
780 INPUT F
790 FIND F
800 INPUT @33:N$
810 INPUT @33:G
820 INPUT @33:A1,A2
830 INPUT @33:Y
840 PRINT N$
850 PRINT "DIVIDE BY?"
860 INPUT D
870 Y=Y/D
880 PRINT "RAW OSEE?"
890 INPUT F
900 PRINT "SHIFT HOW MANY?"
910 INPUT P

```



```

920 FIND F
930 INPUT @33:IN
940 INPUT @33:IC
950 INPUT @33:A1,A2
960 INPUT @33:Z
970 FOR I=1 TO 8
980 IF I+P>0 THEN 1010
990 W(I)=X(I)*Z(I)/Y(I)
1000 GO TO 1030
1010 IF I+P>8 THEN 990
1020 W(I)=X(I+P)*Z(I)/Y(I+P)
1030 NEXT I
1040 PRINT "FILE?"
1050 INPUT G
1060 PRINT "DATA SET NAME?"
1070 INPUT W$
1080 FIND G.
1090 IF TYP(0)<>0 THEN 1190
1100 FIND G
1110 MARK 1,80+179*18
1120 FIND G
1130 PRINT @33:W$
1140 PRINT @33:S
1150 PRINT @33:A1,A2
1160 PRINT @33:W
1170 CLOSE
1180 RETURN
1190 PRINT "FILE "G" IS NOT NEW!"
1200 RETURN

```

APPENDIX 6

TEMPERATURE CONTROLLER

The temperature control circuit was designed to provide a linear heating rate and presettable upper limit in the range 0 to 400°C. In addition this circuit provides zero voltage switching of the heater in order to minimize RF noise generation. Linear heating is accomplished by accumulating clock pulses in a binary counter and supplying the output from the counter to a digital-to-analog converter (DAC). The output of the DAC is a linearly increasing voltage which is compared to the temperature of the sample by a differential amplifier (see Figure 33) and the resulting error signal drives a monolithic zero voltage switch (ZVS). The ZVS supplies energy to the AC heater in proportion to the error signal, with the added advantage that the heater is turned on or off only when the line voltage passes through zero, thus prolonging the life of the heater and eliminating the generation of spurious RF noise.

The thermal emf of a chromel-alumel thermocouple is amplified by a 308 operational amplifier with a gain of 570 as shown in Figure 34. A voltage divider composed of R_5 , R_6 , and R_7 in the second amplifier stage forms a "zero" control for the temperature sensor. This gives an output of about 10 volts when the thermocouple is at a temperature of 400°C. A voltage divider consisting of R_8 and R_9 drops this output into the range of a 0 to 0.1 volt digital volt meter (DVM). R_9 is

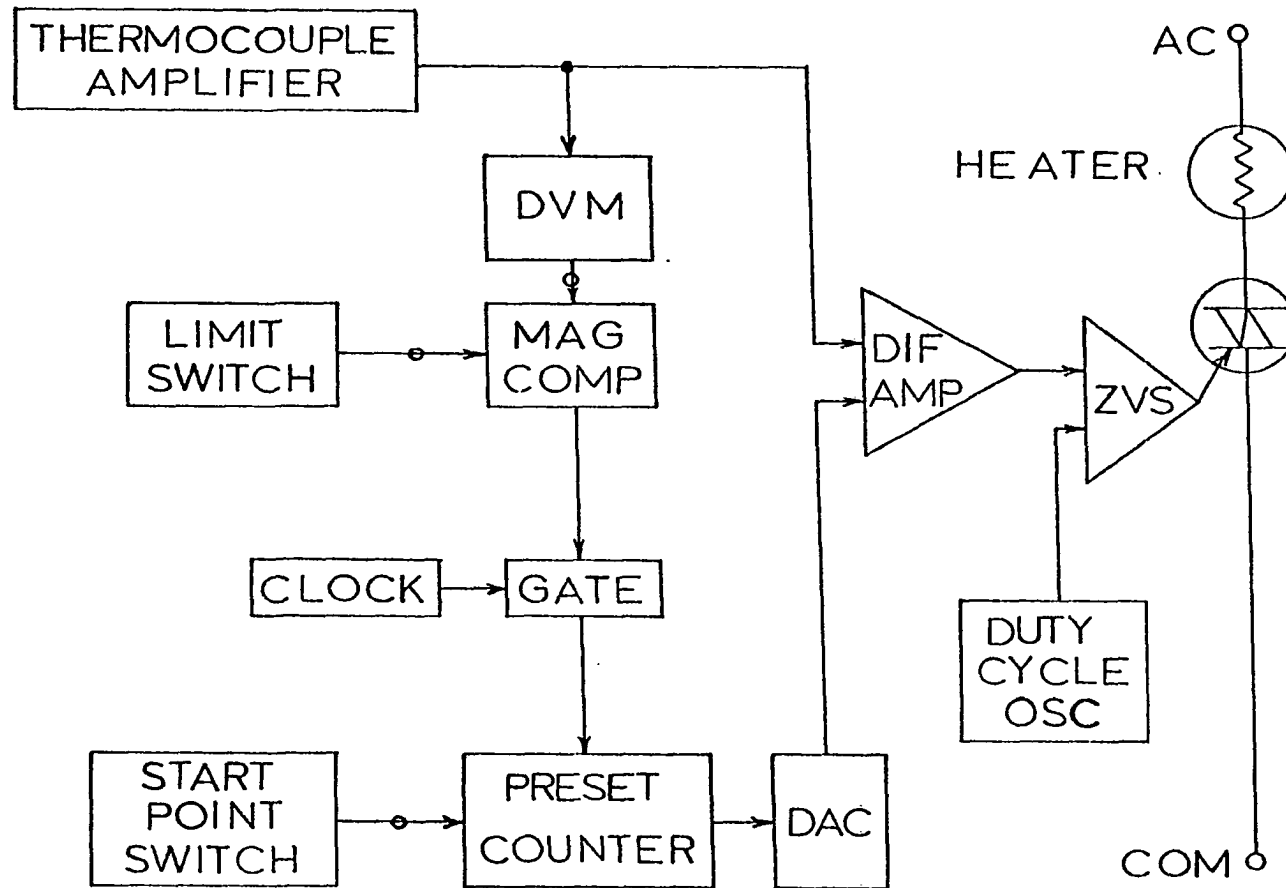


Figure 34. Temperature Controller Block Diagram.

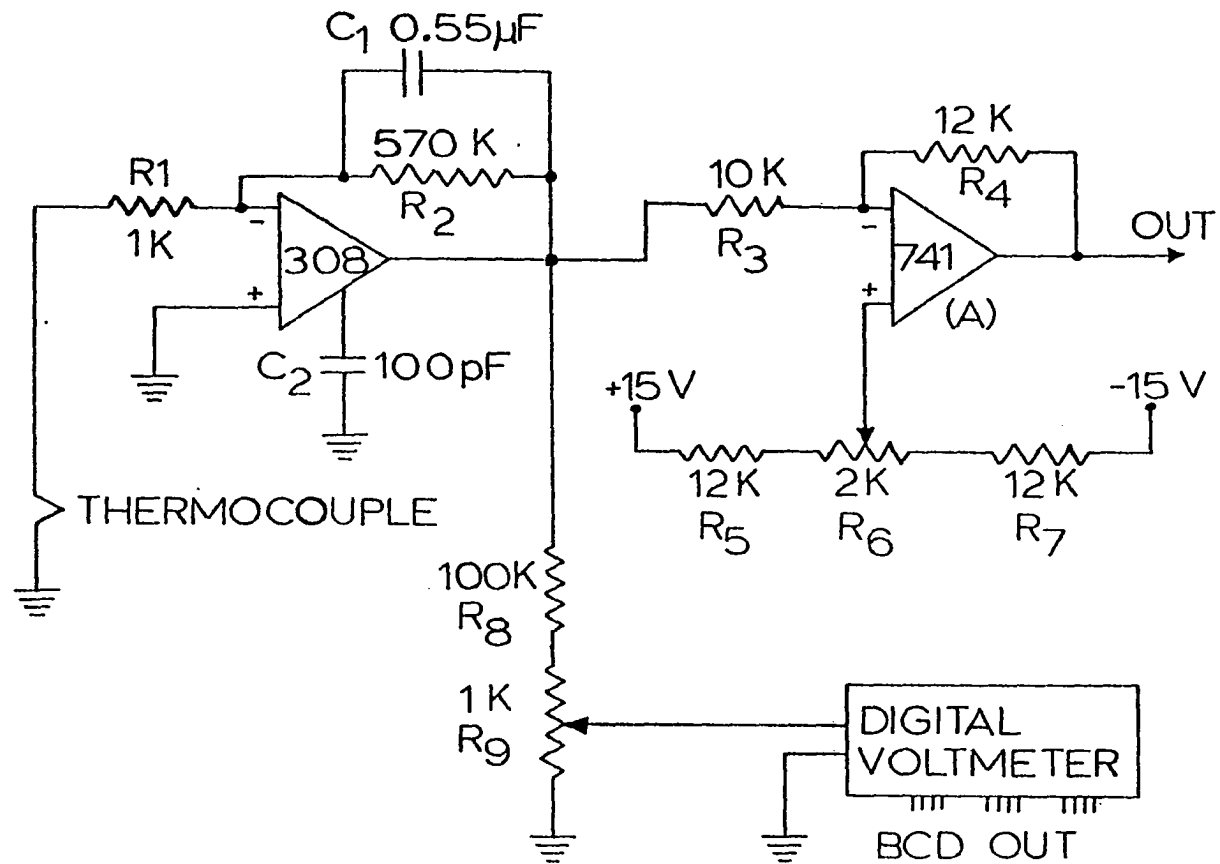


Figure 35. Thermocouple Amplifier Circuit.

adjusted so that when the thermocouple is at 400°C the DVM reads 0.04 volts, thus the meter reads temperature directly except for the non-linearity of the thermocouple. The DVM is equipped with a binary coded decimal (BCD) output so that the temperature of the sample at any given time can be supplied in digital form to the control circuit.

A reference voltage, V_r , is supplied to the DAC by means of a voltage divider composed of R_1 , R_2 , and R_3 as shown in Figure 35. V_r is the maximum voltage which will appear at the output of the DAC when all 12 of the input ports are held at logical 1. The DAC divides V_r into 2^{12} (=4096) equal parts and its output voltage at any given time is that fraction of V_r which is represented by the binary number coded onto its input ports. These input ports are connected to the outputs of three presetable four-bit binary counters (74193). The three counters are cascaded together and used to count pulses from a variable frequency pulse generator. Thus the linearity of the ramp depends only upon the stability of the pulse generator, and the slope of the ramp is determined by the frequency of the pulse generator. The maximum slope obtainable is limited by the power of the heater used and the thermal inertia of the system being heated.

The fact that the binary counters are presetable allows the heating rate cycle to begin at any point in the 0 to 400°C range by simply coding the starting point voltage in binary form onto the input switches. This eliminates the necessity of always starting the heating cycle at 0°C and waiting for the heat rate signal to reach room temperature before the heater turns on.

The particular DAC used in constructing the instrument described

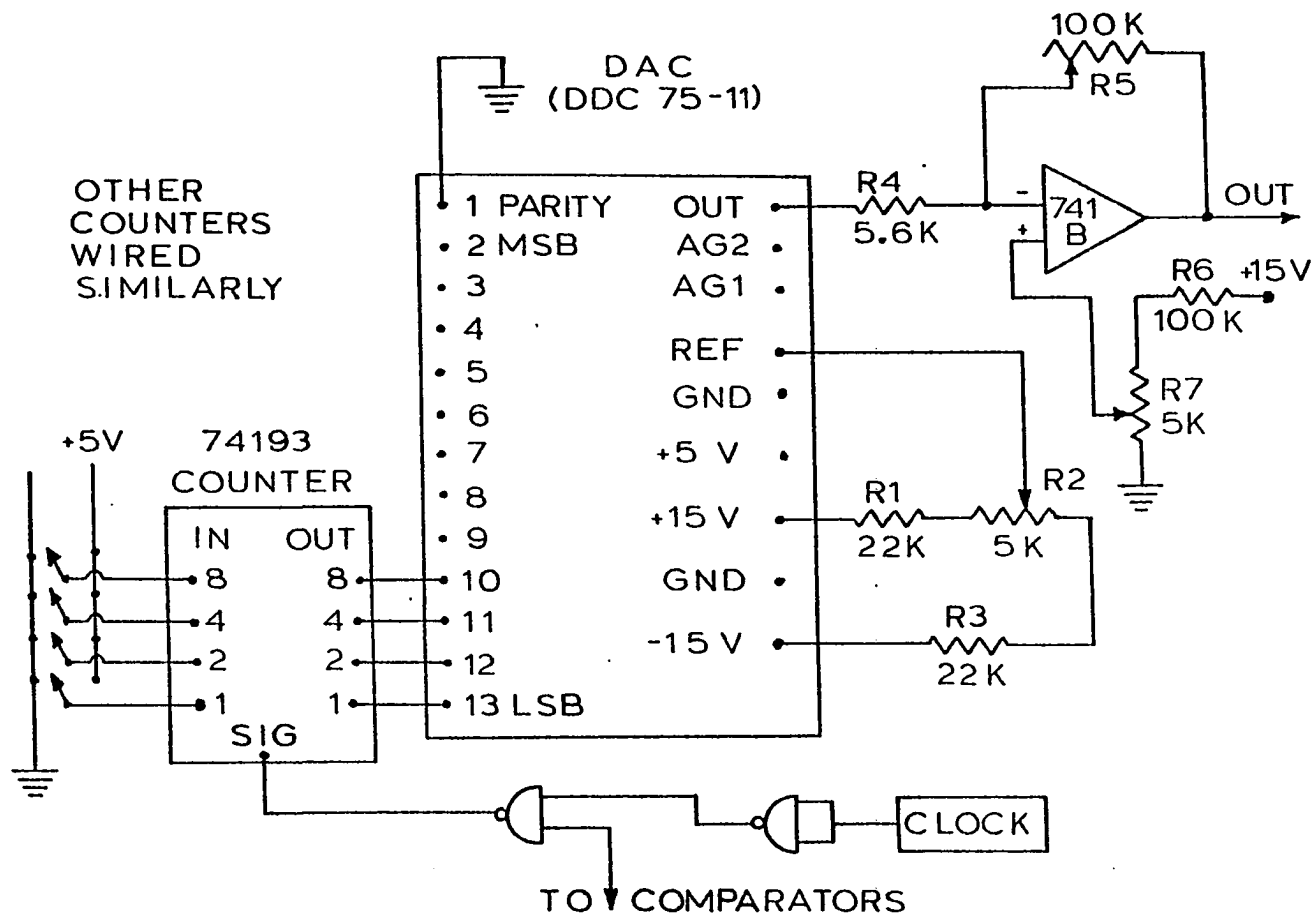


Figure 36. Linear Ramp Circuit.

here possesses the ability to deliver voltages that fall in either of two ranges, 0 to $-V_r$ or 0 to $+V_r$, depending on the logical state of its parity bit. In order to protect the DAC from either a current or voltage overload it was operated in its negative going mode with a maximum output voltage of -0.5 volts. The output was then inverted and amplified by a 741 operational amplifier (B) to provide the heating rate signal to the differential amplifier.

To stop the temperature of the sample from increasing and maintain it at some fixed value, it is only necessary to stop supplying clock pulses from the pulse generator to the binary counters. To accomplish this automatically at some preset temperature, the clock pulses are inverted and then re-inverted by two NAND gates before supplying them to the counters. The second NAND gate not only inverts the pulses, but it also allows them to pass only so long as its secondary input is held high. This gating input is held high only if the temperature of the sample is less than the preset upper limit. When the preset limit is reached the gate goes low and no more clock pulses can reach the counters; therefore heating ceases, and the controller functions only to maintain the set temperature.

This gating signal is derived from the output of three 7485 four-bit magnitude comparators cascaded together. The B inputs of the comparators are supplied by the BCD outputs of the DVM that is used to indicate the temperature of the sample. These inputs are compared bit by bit to the upper limit values presented at the A inputs of the comparators, and a logical 1 appears at pin 5, 6, or 7 of the third comparator depending upon whether $A > B$, $A = B$, or $A < B$ respectively. If the gating input

of the NAND gate is connected to the A>B output of the comparators (pin 5) then clock pulses will pass to the counters until the DVM reads the value that is coded into the upper limit switches.

The zero voltage switch used to translate the error signal into proportional power control is an integrated circuit device (RCA CA3059) which consists of a zero-crossing detector, a differential on/off sensing amplifier, and a triac gating circuit. In normal operation the ZVS compares the voltages presented to two inputs (pins 9 and 13) if $V_{13} > V_9$ a pulse train will be presented at the output (pin 4) to fire a triac each time the AC line voltage passes through zero volts. When V_{13} becomes less than or equal to V_9 the pulse train ceases and the heater is off.

The method of obtaining proportional control from the CA3059 is described in detail in RCA Applications Note ICAN-6168 and the circuit shown in Figure 36 is essentially the same as described in that note. Some parts substitutions were made because of availability. The one transistor oscillator formed by Q_1 produces a sawtooth wavetrain which establishes a duty cycle for the heater. At any instant of time the sawtooth voltage applied to pin 9 is compared with the error signal applied to pin 13. As long as the error voltage is greater than the voltage of the sawtooth generator the ZVS is on and the heater receives 120 VAC. As soon as the sawtooth voltage rises above the error signal, however, the ZVS switches off and the heater receives no power for the remainder of the duty cycle. Therefore the heater is always either completely on or completely off. However the power to the heater is proportioned in time so that the heater is on only for the fraction of

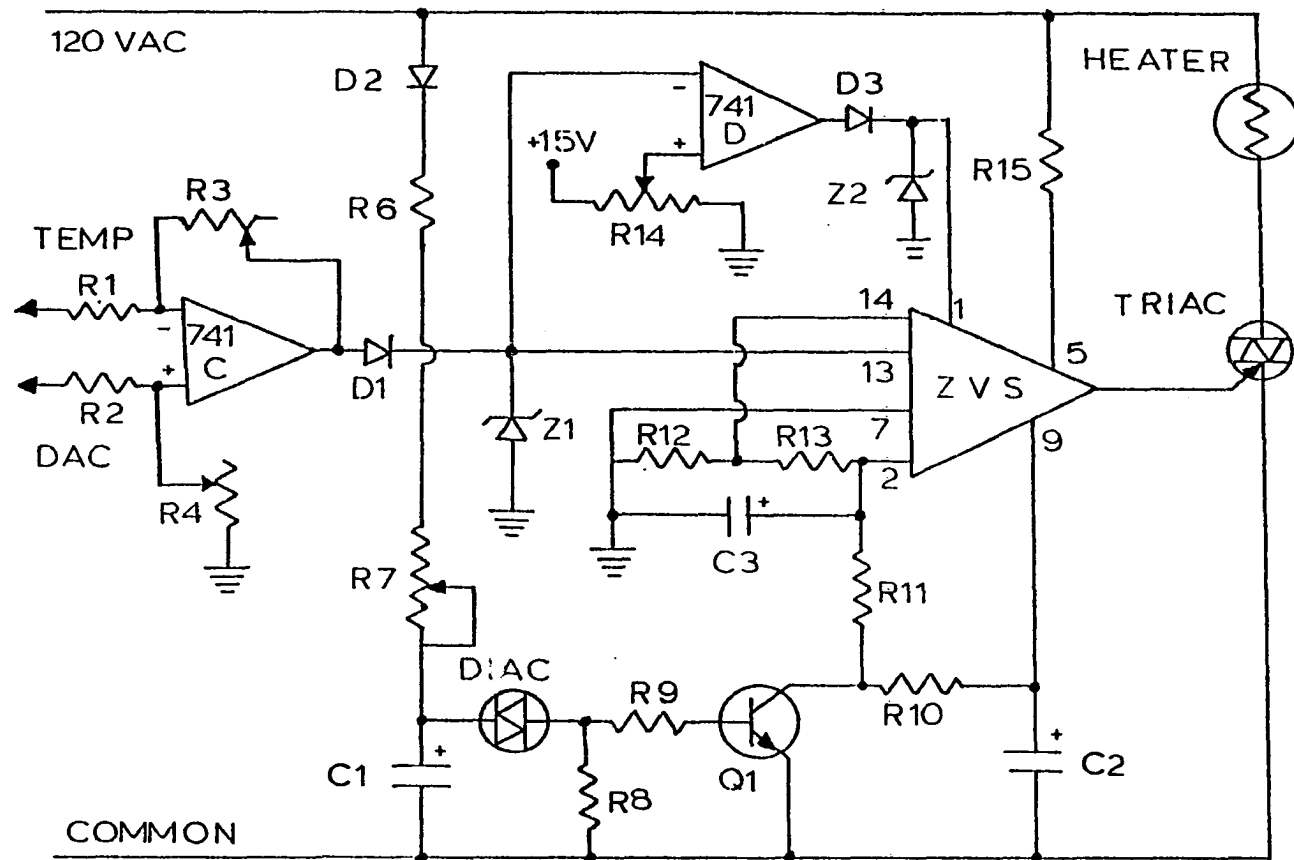


Figure 37. Zero Voltage Switch Circuit.

the duty cycle that is proportional to the error signal.

Two peculiarities of the ZVS had to be overcome in order to obtain proper operation. If the protection input (pin 14) is connected to the error signal input as suggested in the applications note then when the error signal becomes larger than about 4.7 volts the ZVS shuts off. It is therefore necessary to establish pin 14 at about 3 volts by means of R_{12} and R_{13} . Also if the error signal ever becomes smaller than the minimum value of the sawtooth generator then the ZVS will remain on continuously instead of shutting off as desired. To avoid this problem a 741 operational amplifier (D) is used as a voltage comparator to provide an inhibit signal to the ZVS if the error voltage goes lower than the potential set by R_{14} .